Aerosol-Assisted Chemical Vapour Deposition of ZnS from Thioureide Single Source Precursors

Hannah S. I. Sullivan,[a] James D. Parish,[a] Prem Thongchai,[a] Gabriele Kociok-Köhn,[b] Michael S. Hill,[a] and Andrew L. Johnson[a]*

[a]. *Department of Chemistry, University of Bath, Claverton Down, Bath, BA2 7AY, UK.*

[b]. *Materials and Chemical Characterisation Facility (MC^2), Department of Chemistry, University of Bath. Claverton Down, Bath, BA2 7AY, UK.*

Email: a.l.johnson@bath.ac.uk

KEYWORDS: Zinc, thiourea, single source precursor, Aerosol-Assisted CVD, thin film.

ABSTRACT: A family of twelve Zinc(II) thoureide complexes, of the general form [{**L**}ZnMe], [{**L**}Zn{N(SiMe$_3$)$_2$}] and [{**L**}$_2$Zn], have been synthesized by direct reaction of the thiourea pro-ligands ^{i}PrN(H)CS(NMe$_2$) H[**L^1**], CyN(H)CS(NMe$_2$) H[**L^2**], ^{t}BuN(H)CS(NMe$_2$) H[**L^2**] and MesN(H)CS(NMe$_2$) H[**L^4**] with either ZnMe$_2$ (1:1) or Zn{N(SiMe$_3$)$_2$}$_2$ (1:1 and 2:1) and characterised by elemental analysis, NMR spectroscopy and thermogravimetric analysis (TGA).

The molecular structures of complexes [{**L**^{1}}ZnMe]$_2$ (**1**), [{**L**^{2}}ZnMe]$_2$] (**2**) [{**L**^{3}}ZnMe]$_\infty$ (**3**), [{**L**^{4}}ZnMe]$_2$] (**4**), [{**L**^{1}}Zn{N(SiMe$_3$)$_2$}]$_2$ (**5**), [{**L**^{2}}Zn{N(SiMe$_3$)$_2$}]$_2$ (**6**), [{**L**^{3}}Zn{N(SiMe$_3$)$_2$}]$_2$] (**7**), [{**L**^{4}}Zn{N(SiMe$_3$)$_2$}]$_2$] (**8**), [{**L**^{1}}$_2$Zn]$_2$ (**9**) and [{**L**^{4}}$_2$Zn]$_2$ (**12**) have been unambiguously determined using single crystal X-ray diffraction studies. Thermogravimetric analysis has been used to assess the viability of complexes **1**-**12** as single source precursors for the formation of ZnS. On the basis of TGA data compound **9** was investigated for its utility as a single source precursor to deposit ZnS films on silica-coated glass and crystalline silicon substrates at 150, 200, 250 and 300 °C using an aerosol assisted chemical vapour deposition (AACVD) method. The resultant films were confirmed to be hexagonal-ZnS by Raman spectroscopy and PXRD, and the surface morphologies were examined by SEM and AFM analysis. Thin films deposited from (**9**) at 250 and 300 °C were found to comprise of more densely packed and more highly crystalline ZnS than films deposited at lower temperatures. The electronic properties of the ZnS thin films were deduced by UV–Vis spectroscopy to be very similar and displayed absorption behaviour and band gap (E_g = 3.711-3.772 eV) values between those expected for bulk cubic-ZnS (Eg = 3.54 eV) and hexagonal-ZnS (Eg = 3.91 eV).

Introduction

As one of the first semiconducting materials to be discovered, zinc sulfide (ZnS) is the prototype II–VI semiconductor, and has habitually displayed remarkable fundamental properties and versatility of application, finding utility in a wide range of areas such as electronics and optoelectronics, photovoltaic cells, optical sensors, lasers, infrared windows, electroluminescent and photo-luminescent devices, antireflection coatings, reflectors, interference filters and displays.[1]

Understanding the relationship between structural and electronic properties of semiconducting materials is crucial to the design of novel nanostructures with tunable properties. Zinc sulfide exists in three polymorphic forms:[2] cubic zinc blende (ZB-ZnS, also called β-ZnS or "sphalerite"), hexagonal Wurtzite (W-ZnS), or the rarely observed cubic rock salt (RS-ZnS),[3] with each phase possessing unique physical properties.[4] In both cubic and hexagonal structures, Zn and S atoms exist in tetrahedral environments, where the only difference is in the stacking sequence of atomic layers. A consequence of this difference in the physical arrangement of the atoms within the lattice is the difference in band-gap energy observed for ZB-ZnS (Eg = 3.54 eV) and W-ZnS (Eg = 3.91 eV).[2]

Zinc sulfide is generally considered one of the best materials available as a buffer layer for the fabrication of CIGS solar cells. ZnS provides a non-toxic and environmentally safe alternative to cadmium sulfide, and displays improved lattice matching to CIGS absorbers in addition to being capable of transmitting higher energy photons and increasing light absorption in the absorber layer (*cf.* CdS).[5]

A wide range of thin film deposition techniques[6] have been applied to the fabrication of ZnS thin films. From a commercial and technological viewpoint, many of these techniques entail high

operating cost and often require complicated operational steps and instrumentation, without the guarantee of high reproducibility. As such, studies have focused on routes by which high quality ZnS thin films can be produced at low cost in a consistent and reproducible manner.

To this end, a variety of metalorganic complexes of zinc (including dialkyldithiocarbamates,[1d, 7] alkyl xanthates,[8] thiosemicarbazones,[9] dialkylthiocarbamtes and monothiocarboxylates,[10] dithiophosphinate11 N-thiophosphorylated-thioureas[12] and thio- and dithio-biuret[13]) have been designed and developed for application in the chemical vapour deposition (CVD) of ZnS thin films.[14] Reviews by Gleizes[15] and O'Brien[14b, 16] provide detailed accounts of the use of other single source precursors for the deposition of chalcogenide materials by MOCVD. Of these precursors, $[Zn(S_2CNEt_2)_2]$ was the first precursor compound employed, yielding only poor quality ZnS via a low-pressure CVD (LP-CVD) process. Reports suggest that the implementation of $[Zn(S_2CNEt_2)_2]$ in other thin film deposition methods can produce good quality hexagonal and cubic ZnS films on Si(111) substrates[17] and, in related studies, nanocrystalline W-ZnS thin films have been deposited on crystalline silicon and silicon dioxide substrates by CVD from $[Zn(S_2COR_2)_2]$(R = Et or ^{i}Pr).[8a, 8c]

Many of these systems, however, suffer from inconveniently low precursor volatility unless used at very low pressures.[14b, 15, 18] An alternative variant on the CVD technique, which circumvents this limitation and avoids the use of highly reactive metal alkyls or H_2S, is aerosol-assisted CVD (AACVD),[19] where the only restriction on precursor identity in this respect is its solubility in appropriate solvents, with the subsequent solutions nebulized and transported as micron-scale droplets to a heated substrate.[18, 20] Despite its obvious advantages, however, only the monothiocarboxylate complexes $[Zn(SOCMe)_2(tmeda)]$ and $[Zn(SOC^tBu)_2(tmeda)]$ (tmeda = N,N,N,N-tetramethylethylenediamine), and the tetramethyl-dithiobiurete complex

[Zn{(SC(NMe$_2$))$_2$N}$_2$] have been utilized in AACVD studies to date. The former of these two complexes produced thin films in which mixtures of ZB-ZnS and W-ZnS were observed at temperatures as low as 125 °C,[10a] whilst the latter deposited ZB-ZnS below 350 °C and W-ZnS at deposition temperatures above 400 °C.[13a, 14b]

Recently we described the design and synthesis of metal precursors based around thioamidate[21] and thioureide[22] ligand systems for the production of metal sulfide thin films by AACVD processes. In the present work, we describe the synthesis and characterization of a family of twelve homo- and heteroleptic zinc-thioureide complexes, which have been synthesized by direct reaction of the free thioureates with either ZnMe$_2$ (1:1) or Zn{N(SiMe$_3$)$_2$}$_2$ (1:1 and 2:1). We also report the potential of selected complexes to act as single source precursors to thin films of ZnS.

Results and Discussion

Synthesis

The thiourea pro-ligands, H**L^1**-H**L^4**, were prepared by direct reaction of the appropriate commercially available isothiocyanates with anhydrous HNMe$_2$ in hexane (Scheme 1), followed by isolation by filtration, washing with fresh hexane, and drying in-vacuo to yield the pure pro-ligands as colorless microcrystalline powders in high yields (81-86 %). In all cases, the products were characterized by solution state NMR (^{1}H and ^{13}C) spectroscopy and elemental analysis.

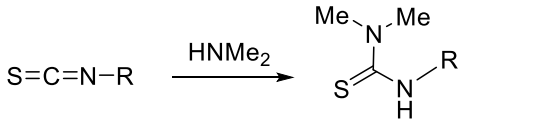

R = ^{i}Pr : H[**L^1**]
R = Cy : H[**L^2**]
R = ^{t}Bu : H[**L^3**]
R = C$_6$Me$_3$H$_2$: H[**L^4**]

Scheme 1

The ^{1}H NMR spectra of the pro-ligands all display a resonance ca. δ 4.42-5.64 ppm associated with the {NMe_2} functionality, a feature which is absent from the starting thioisocyanates, whilst the $^{13}C\{^{1}H\}$ NMR spectra demonstrate a characteristic shift in the resonance associated with the thioisocyanates' {S=C=N} carbon resonance from δ 129-134 ppm to δ 182-183 ppm for the {C═S} double bonds.

The zinc thioureide derivatives, compounds **1-4** and **5-8**, were readily synthesized through the reaction in hexane of 1 equivalent of either [$ZnMe_2$] or [$Zn\{N(SiMe_3)_2\}_2$] with the pro-ligands H**L**^{1}, H**L**^{2}, H**L**^{3} and H**L**^{4} and were isolated as colorless solids (Scheme 2).

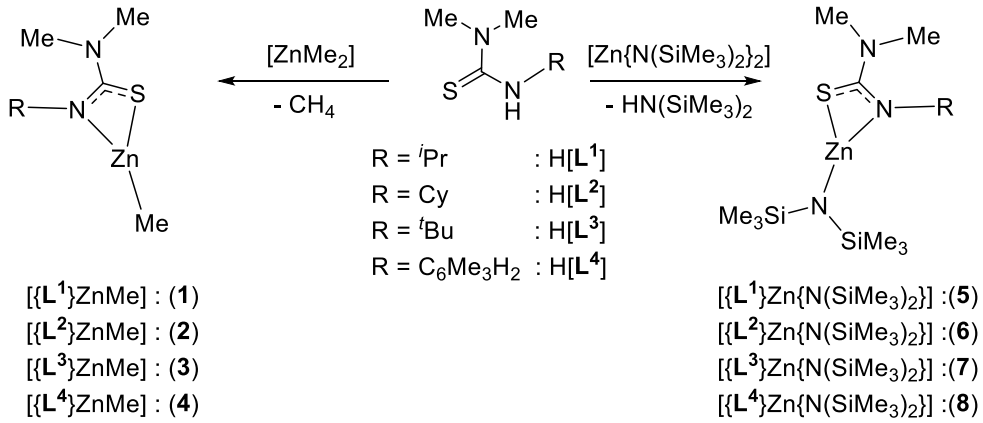

Scheme 2

The reaction of both [$ZnMe_2$] and [$Zn\{N(SiMe_3)_2\}_2$] with the pro-ligands H**L**^{1}-H**L**^{4} in a stoichiometric 1 : 1 reaction results in the formation, and isolation after recrystallization, of the mono-thioureide complexes **1-4** and **5-8**, respectively. The ^{1}H NMR spectra clearly show the absence of the broad singlet resonance associated with the {NH} group in the pro-ligands, indicating loss of this acidic proton as either CH_4 or $HN(SiMe_3)_2$. In the case of complexes **1**, **2** and **4**, and **5-8**, the complexes are all soluble in C_6D_6 whereas in contrast, complex **3** displayed

limited solubility in C_6D_6, suggestive of subtle differences between the solution state structures of complex **3** and **7**. Despite this observation, the ^{1}H NMR spectra of the respective compounds clearly show the presence of singlet resonances at δ = -0.01 ppm, (**1**), 0.05 ppm, (**2**), 0.01 ppm, (**3**), and 0.41 ppm, (**4**), representative of the {Zn-Me} moiety in compounds **1-4**, and at δ = 0.46 ppm (**5**), 0.46 ppm (**6**), 0.44 ppm (**7**) and 0.31 ppm (**8**) in compounds **5-8**, representative of a {Zn-N(SiMe$_3$)$_2$} moiety. These resonances appear in relative ratios of 3H:6H and 18H:6H respectively, with the dimethylamine group, {NMe$_2$} of the ligands {**L^1**}-{**L^4**}, indicative of the presence of the thioureide ligand and {Me}, or {N(SiMe$_3$)$_2$} groups in a 1:1 ratio as expected for the formation of the heteroleptic methyl-zinc thiouride complexes **1-4** and the amide zinc thiouride complexes **5-8** (Scheme 2). Elemental analyses of the products are consistent with the formation of the heteroleptic complexes [{L}ZnMe], **1-4** and [{L}Zn-N(SiMe$_3$)$_2$)], **5-8** respectively.

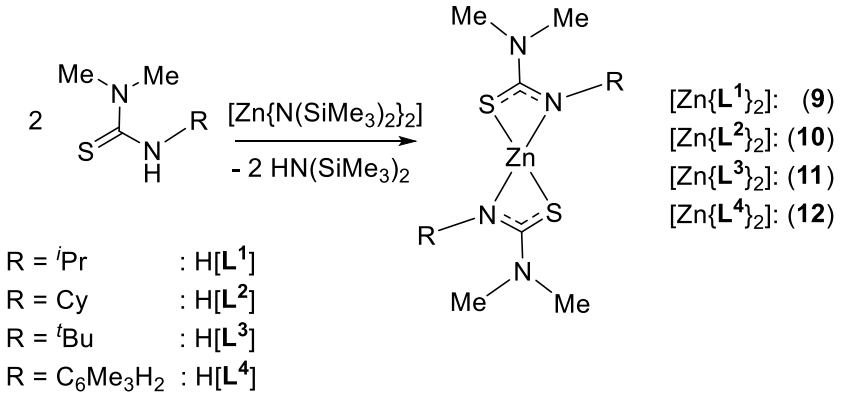

Scheme 3

Comparable reaction of the pro-ligands H**L^1**-H**L^4** with [Zn{N(SiMe$_3$)$_2$}$_2$] in a 2:1 ratio results in the formation of the *bis*-thioureide complexes, **9–12**, in moderate to high isolated yields (56-83%). In contrast to the ^{1}H NMR spectra of **5-8**, the ^{1}H NMR spectra of **9–12** clearly show the absence of resonances associated with the {N(SiMe$_3$)$_2$} units (ca. 0.31-0.48 ppm) and are consistent with

the formation of the *bis*-thioureide complexes (Scheme 3). The appearance of only one set of resonances in the ^{1}H and ^{13}C NMR spectra for the thioureide ligands in all four sets of spectra is indicative of the fact that that the ligands occupy identical environments on the NMR timescale. Elemental analysis of **9-12** is consistent with the formation of the *bis*-thioureide complexes.

Solid State Molecular Structures

X-ray quality single crystals of compounds **1-4**, **5-8, 9** and **12** were obtained from a saturated toluene solution at −28 °C. Figure 1 shows the molecular structure of compounds **1**, **2** and **4**, which present as an essentially iso-reticular series consisting of dimeric molecular units, [{**L**}ZnMe]$_2$.

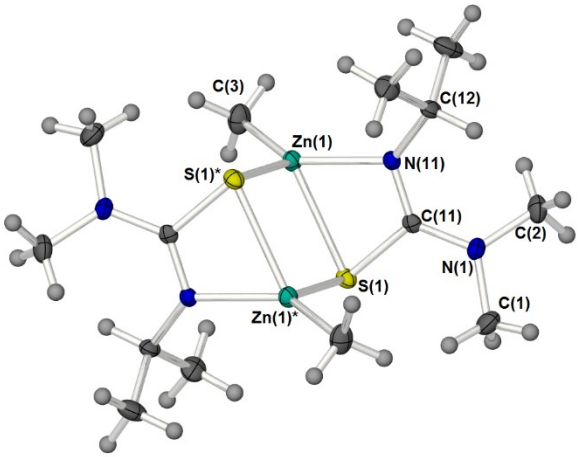

Figure 1: Molecular structure of [{**L**^{1}}ZnMe]$_2$ (**1**). Thermal ellipsoids are shown at 50% probability. Symmetry transformations used to generate equivalent atoms: -X+1,-Y,-Z+1.

Complex **1**, which crystallizes in the monoclinic space group P2$_1$/n, forms a centrosymmetric dimer with anti-arrangement of the thioureide ligands about the central {Zn_2S_2} metallocycle, similar to the amidinate and dithiocarbamate systems [{^{t}BuC(N*i*-Pr)$_2$}ZnMe]$_2$[23] and [{Et_2NCS_2}ZnMe]$_2$.[7b] Each thioureide ligand can be best described as being coordinated to the

zinc centers in a $\mu,\kappa^2:\kappa^1$ coordination mode, i.e. η^2-N,S-chelating fashion to one zinc center, while participating in a S-bridging interaction with an adjacent zinc center. Whilst each zinc atom in the series of complexes is four coordinate, the coordination at the metal is not simply described in terms of any regular polyhedron. In the case of complex **1**, the geometry about the zinc atoms is best described as distorted trigonal pyramidal, with the base defined by the atoms C(3), N(11) and S(l)* [$\sum_{Zn}$ = 354.54(6)°]. Coordination of the sulfur atom from the chelating thioureide, Zn-S_{int} [2.5348(7) Å], which is significantly longer than the dimer-forming exocyclic Zn-S^*_{exo} interaction [2.4474(7) Å], completes the coordination environment and distorts the geometry away from ideal due to the restricted S(1)-Zn(1)-N(11) bite angle [68.10°]. The Zn-Me bond [1.970(3) Å] is similar to those found in related complexes.[7b] The C–S bond length [1.775(3) Å] is close in value to that expected for typical C–S single bonds, whereas the C–N bond [1.362(3) Å] is more consistent with its assignment as a localized C═N double bond. Despite the approximate co-planarity of the {CNS} and {NMe_2} moieties (the angle between the two planes is ~27.79°) within the thioureide ligand, there is no evidence of multiple bonding character between {CNS} and {NMe_2} groups, as indicated by the approximately single C-N bond [1.301(3)Å]. The same general trends observed in complex **1** are repeated in complexes **2** and **4**. Table 1 shows selected bond lengths and angles for complexes **1**, **2** and **4** and their molecular structures are shown in Figure 2.

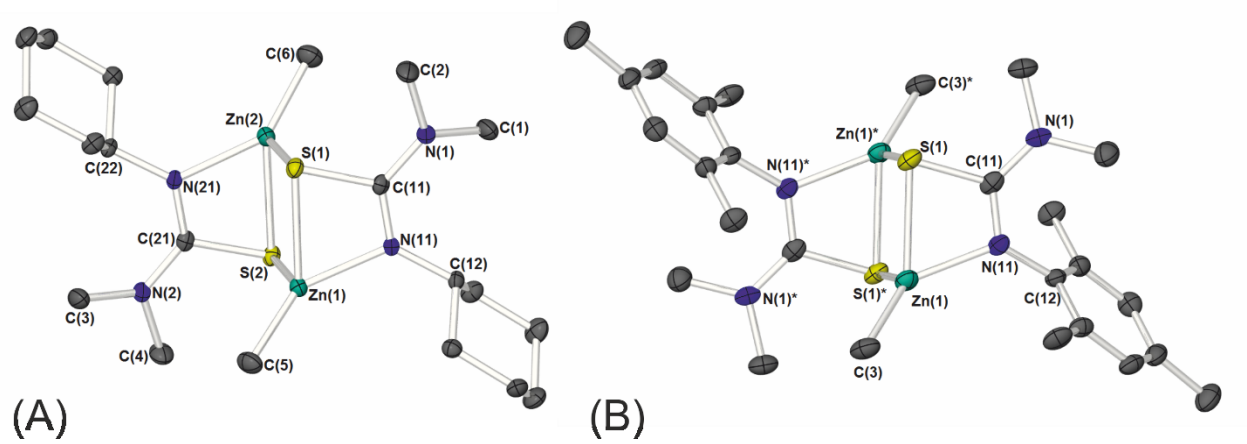

Figure 2: Molecular structure of A: [{$\mathbf{L^2}$}ZnMe]$_2$ (**2**) and B: [{$\mathbf{L^4}$}ZnMe]$_2$ (**4**). Thermal ellipsoids are shown at 50% probability. Hydrogen atoms have been omitted for clarity. Symmetry transformations used to generate equivalent atoms in B: -X+1,-Y+1,-Z.

Table 1: Selected bond lengths (Å) and bond angles (°) for complexes **1, 2** and **4**.

	1	**2**	**4**
Zn–Me	1.970(3) Å	1.963(2) Å & 1.968(2) Å	1.965(4) Å
Zn–S_{int}	2.5348(7) Å	2.5295(6) Å & 2.5374(6) Å	2.5217(10) Å
Zn–N	2.036(2) Å	2.0261(16) Å &2.0253(16) Å	2.046(3) Å
Zn–S_{exo}	2.4474(7) Å	2.4447(5) Å & 2.4493(5) Å	2.4748(10) Å
C–NMe_2	1.362(3) Å	1.354(3) Å & 1.354(3) Å	1.350(4) Å
S–C	1.775(3) Å	1.7821(19) Å & 1.7834(19) Å	1.788(3) Å
N–C	1.301(3) Å	1.308(3) Å & 1.308(3) Å	1.307(4) Å
S–Zn–N	68.10(5)°	68.20(5)° & 67.85(5)°	68.20(8)°

In stark contrast to the molecular structures of complexes **1**, **2** and **4**, the solid state structure of **3**, containing the sterically more demanding ^{t}Bu group, adopts a rather unexpected structure in the solid state, favouring the formation of a polymeric system in which the coordination mode of the thioureide moiety differs significantly to that observed in **1**, **2** and **4**. The molecular structure of complex **3** is shown in Figure 3 and selected bond lengths and angles in Table 2.

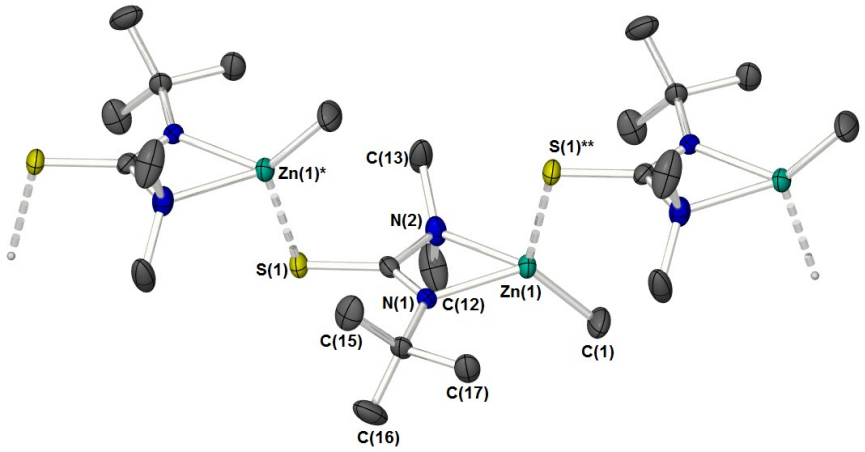

Figure 3: A projection along the c axis showing both the molecular structure of [{$\mathbf{L^3}$}ZnMe]$_\infty$ (3) and the formation of the one dimensional polymeric chains. Thermal ellipsoids are shown at 50% probability. Hydrogen atoms have been omitted for clarity. Symmetry transformations used to generate equivalent atoms in 3: * -X+1,Y+1/2,-Z+3/2; ** -X+1,Y-1/2,-Z+3/2.

Table 2: Selected bond lengths (Å) and bond angles (°) for complex **3**.

	3
Zn–Me	1.968(3) Å
Zn–N^{t}Bu	2.090(2) Å
Zn←NMe$_2$	2.203(2) Å
Zn···S	2.3540(8) Å
C–NMe$_2$	1.472(4) Å
S–C	1.743(2) Å
^{t}BuN–C	1.268(3) Å
^{t}BuN–Zn–NMe$_2$	62.57(9)°
Me-Zn···S	124.54(10)°

Complex **3** crystallizes in the orthorhombic space group $P2_12_12_1$ with one complete molecule in the asymmetric unit cell. The asymmetric units are connected in the form of one-dimensional zig-zag polymeric chains extended along the crystallographic *a*-axis. As with complexes **1**, **2** and **4** the zinc metal center possesses a 4-coordinate geometry. Unlike **1**, **2** and **4**, however, the coordination

environment is made up of the two nitrogen atoms of the thioureide ligand, the carbon of the terminal {Me} group and the {S} atom of an adjacent [{$\mathbf{L^3}$}ZnMe] unit. This contrasting κ^2-*N*,*N*′ coordination mode of the thioureide ligand is comparable to that observed in the related ureide-coordinated complex [Sn{κ^2-*N*,*O*-OC(NMe$_2$)N^{t}Bu}{κ^2-*N*,*N*′-N(^{t}Bu)C(S)NMe$_2$}].[24] The coordination mode of the thioureide ligand in **2** can be best described as being *N*,*N*′-chelating (κ^2) to the zinc atom along with the terminal {C=S} acting as a bridging atom to an adjacent zinc center. The central planar carbon atom of the thioureide ligand is appended by a sulfur atom, with a S-C bond length indicative of significant double character (1.743 Å), in addition to the {N^{t}Bu} and {NMe$_2$} moieties. The carbon-nitrogen bonds at 1.268(3) Å and 1.472(4) Å respectively are approaching values observed for {C=N^{t}Bu}[25] and {C-NMe$_2$}[25b] bonds, indicative of some delocalization of charge across the {S-C-N^{t}Bu} moiety.

The bond angles around the zinc atom in **3** are in the range expected for a more tetrahedral geometry *cf.* **1**, **2** and **4**. The Zn-C bond lengths observed in **3** (1.968(3) Å) are comparable to those described above, and are in the typical range reported for Zn-Me groups.[7b] The Zn-N^{t}Bu (Zn-N = 2.090(2) Å)[25b] and Zn←{NMe$_2$} bond lengths (Zn-N = 2.203(3) Å)[26] are also in the range expected for comparable bonds in literature complexes. The intermolecular Zn···S bond (2.3540(8) Å) is as long as that found in zinc blende (~2.342 Å).[1c]

In the case of the *bis*-trimethylsilyl derivatives **5**-**8**, there is no comparable change in the coordination mode of the thioureide ligand, as the series traverses from ^{i}Pr to Cy, ^{t}Bu and Mes ligand systems. In general, the solid state molecular structures of **5**-**8** possess a comparable structural topology with the κ^2-N,S complexes **1**, **2** and **4**, with the {N(SiMe$_3$)$_2$} group taking the terminal position adopted by the methyl groups. Figure 4 shows the molecular structure of **7** . Selected bond lengths

and angles for complexes **5-8** are shown in Table 3. The molecular structures of **5**, **6** and **8** are shown in the supplementary information.

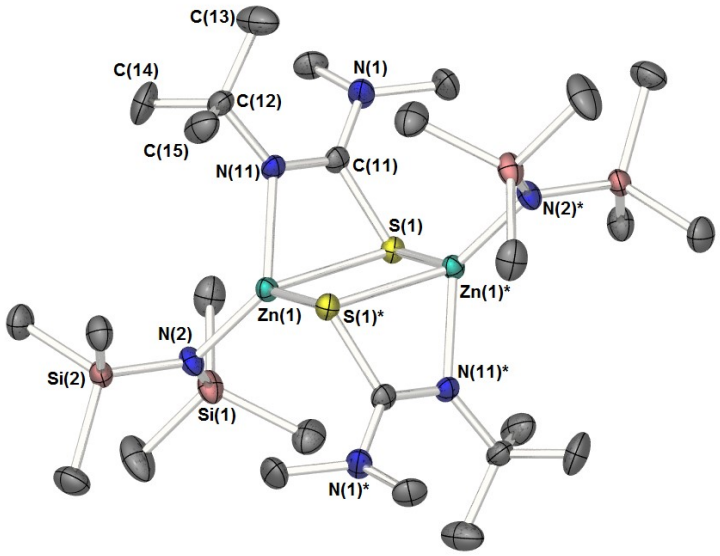

Figure 4: Molecular structure of [{$\mathbf{L^3}$}Zn{$N(SiMe_3)_2$}]$_2$ (**7**). Thermal ellipsoids are shown at 50% probability. Hydrogen atoms have been omitted for clarity. Symmetry transformations used to generate equivalent atoms: -X,-Y,-Z+1.

Table 3: Selected bond lengths (Å) and bond angles (°) for complexes **5-8**.

	5	**6**	**7**	**8**
Zn–$N(SiMe_3)_2$	1.9145(16) Å	1.913(3) Å	1.9141(8) Å	1.9037(14) Å
Zn–S_{int}	2.5363(6) Å	2.5428(12) Å	2.5171(16) Å	2.4970(4) Å
Zn–N	2.0379(17) Å	2.030(3) Å	2.0746(18) Å	2.0278(13) Å
Zn–S_{exo}	2.3871(6) Å	2.3930(11) Å	2.3837(6) Å	2.4282(4) Å
C–NMe_2	1.359(3) Å	1.341(5) Å	1.369(3) Å	1.340(2) Å
S–C	1.785(2) Å	1.785(4) Å	1.801(2) Å	1.7853(16) Å
N–C	1.300(3) Å	1.314(5) Å	1.295(3) Å	1.312(2) Å
S–Zn–N	68.15(5)°	67.98(11)°	68.55(5)°	68.68(4)°

Compound **7** crystallizes in the triclinic space group P-1 with two independent halves of the dimeric compound [{$\mathbf{L^3}$}Zn{$N(SiMe_3)_2$}]$_2$ in the asymmetric unit cell. Complexes **5**, **6** and **8** also crystallize in the triclinic space group P-1, with one half of the respective dimer unit present in the asymmetric unit cells for complexes **5** and **8**, and two independent halves of the dimeric unit in **6**. As with complexes **1**, **2** and **4**, the thioureide ligands in **5**-**8** are coordinated to the zinc centers in a $\mu,\eta^2:\eta^1$-coordination mode and, as with the methyl-zinc complexes described earlier, the molecular structures of **5**-**8** exist as centrosymmetric dimers with an anti-arrangement of ligands about the central $\{Zn_2S_2\}$ metallocycle. The molecular structure of complex **7** is described here as an exemplar with similar features to those observed in complexes **5**, **6** and **8**.

The $\{Zn_2S_2\}$ core of **7** is planar and forms an angle of 77.0° to the equally planar {ZnNCS} metallocycle. As with complex **1**, the geometry about zinc atoms in complexes **5**-**8** is best described as distorted trigonal pyramidal, with the base defined by the atoms N(2), N(11), and S(l)* [$\sum_{Zn}$ = 354.11(6)°] (**5**: $\sum_{Zn}$ = 355.88(5)°, **6**: $\sum_{Zn}$ = 355.55(11)°, **8**: $\sum_{Zn}$ = 347.58(4)°). As in **1**, **2** and **4**, a strong interaction between the two ‘‘monomeric’’ [{$\mathbf{L^3}$}Zn{$N(SiMe_3)_2$}] units is indicated by the shorter Zn-S distance [2.0831(19) Å] compared with Zn-S [2.1879(18) A˚].

Coordination of the sulfur atom from the chelating thioureide, Zn-S_{int} [2.5171(6) Å], which is significantly longer than the dimer forming exocyclic Zn-S*$_{exo}$ interaction [2.3837(6) Å], completes the coordination environment and distorts the geometry away from ideal due to the restricted S(1)-Zn(1)-N(11) bite angle [68.55(5)°].

The remaining Zn-N bond of the chelating {$\mathbf{L^3}$} anion is marginally longer [2.0746(18) Å] than the analogous bonds in compounds **1**, **2** and **4**. The Zn-N amide distance [1.9141(18) Å] is

comparable to the structurally related [{hpp}Zn{N(SiMe$_3$)$_2$}]$_2$ ({hhp} = 1,3,4,6,7,8-hexahydro-2H-pyrimido[1,2-a]pyrimide) in which the zinc geometry is described as distorted tetrahedral.[27]

Single crystals of the *bis*-thioureide complexes **9** and **12** were obtained independently from solutions of toluene upon storage at -28 °C. Complexes **9** and **12** crystallize in the monoclinic space group I2/a and the triclinic space group P-1, respectively. For **9** the asymmetric unit cell contains one [{L^1}$_2$Zn] molecule, alongside one molecule of toluene, with symmetry operators generating the second half of the dimeric [{L^1}$_2$Zn]$_2$ system (Figure 5). Similarly for **12** the asymmetric unit cell contains one complete [{L^4}$_2$Zn] molecule, with symmetry operators generating the second half of the dimeric [{L^4}$_2$Zn]$_2$ system (Figure 5). Table 4 shows selected bond lengths and angles for complexes **9** and **12**.

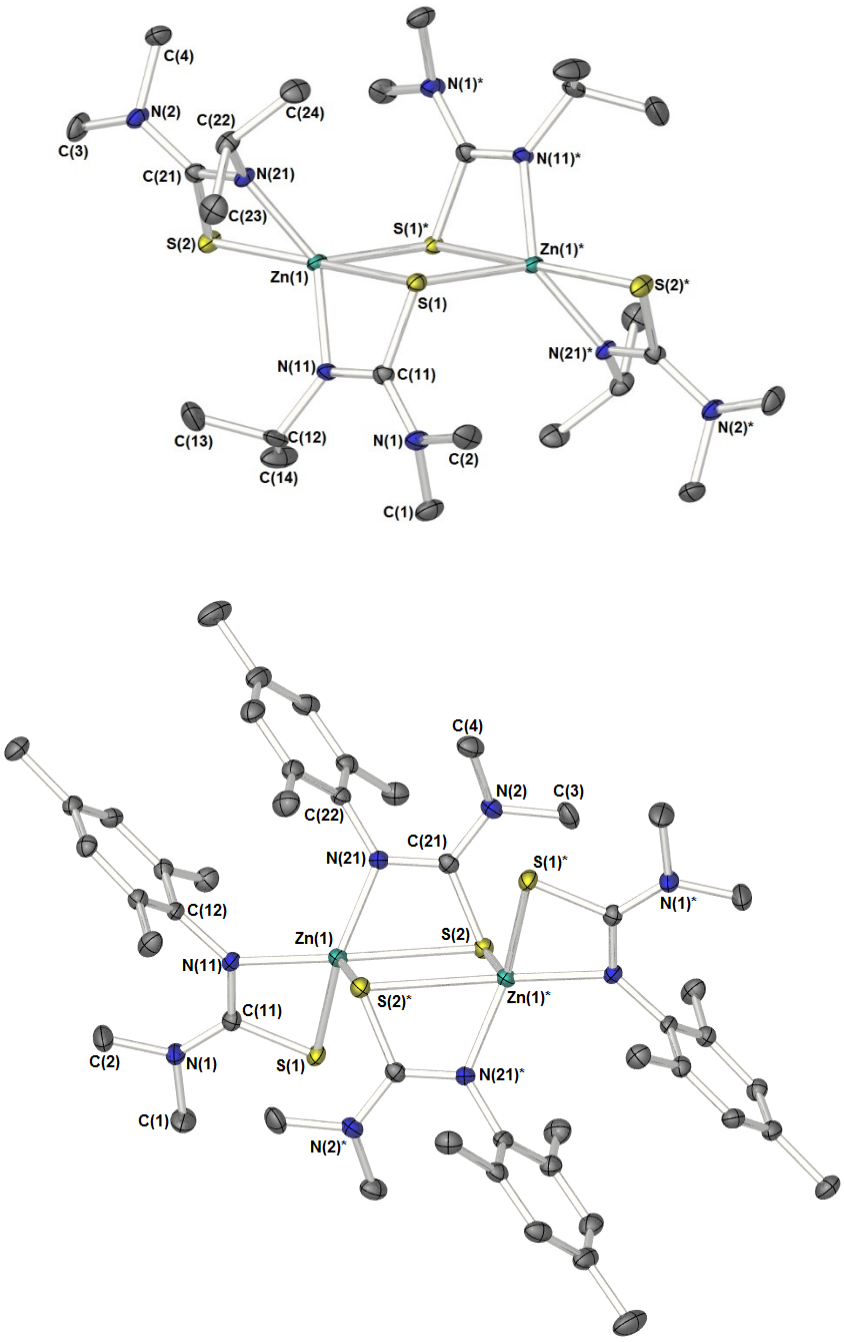

Figure 5: Molecular structure of the *bis*-thioureide complexes [{$\mathbf{L^1}$}Zn]$_2$ (**9**) and [{$\mathbf{L^4}$}Zn]$_2$ (**12**). Thermal ellipsoids are shown at 50% probability. Hydrogen atoms, and solvent of crystallization (toluene) associated with **9** has been omitted for clarity. Symmetry transformations used to generate equivalent atoms: **9**; -X+1/2,-Y+1/2,-Z+1/2, **12**; -X+1,-Y+2,-Z+1.

Table 4: Selected bond lengths (Å) and bond angles (°) for complexes **9** and **12**.

	9		**12**
Zn(1)-S(1)	2.8149(7) Å	Zn(1)-S(1)	2.3764(6) Å
Zn(1)-S(2)	2.4973(7) Å	Zn(1)-S(2)	2.8061(5) Å
Zn(1)-S(1)*	2.3645(7) Å	Zn(1)-S(2)*	2.3666(6) Å
Zn(1)-N(11)	2.0199(19) Å	Zn(1)-N(11)	2.0839(15) Å
Zn(1)-N(21)	2.0174(19) Å	Zn(1)-N(21)	2.0198(17) Å
C(11)–N(1)	1.355(3) Å	C(11)–N(1)	1.352(2) Å
S(1)–C(11)	1.773(2) Å	S(1)–C(11)	1.7529(19) Å
N(11)–C(11)	1.303(3) Å	N(11)–C(11)	1.324(3) Å
C(21)–N(2)	1.376(3) Å	C(21)–N(2)	1.350(3) Å
S(2)–C(21)	1.735(2) Å	S(2)–C(21)	1.756(2) Å
N(21)–C(21)	1.315(3) Å	N(21)–C(21)	1.324(2) Å
S(1)-Zn(1)-N(11)	62.75(6)°	S(1)-Zn(1)-N(11)	70.45(5)°
S(2)-Zn(1)-N(21)	69.03(6)°	S(2)-Zn(1)-N(21)	63.03(5)°
S(1)-Zn(1)-S(1)*	84.85(2)°	S(2)-Zn(1)-S(2)*	89.389(18)°
Zn(1)-S(1)-Zn(1)*	95.15(2)°	Zn(1)-S(2)-Zn(1)*	90.611(18)°

The molecular structures of **9** and **12** are related to those of complexes **1**, **2** and **4**, and **5**-**8**, which have been previously described, and are based on dimeric molecules with highly distorted five-coordinate geometries about each zinc atom, comprising the sulfur and nitrogen atoms of the two chelating thioureide ligands. The fifth, and final, coordinating atom is found to be a sulfur atom belonging to an adjacent chelating thioureide ligand, bridging two zinc atoms and resulting in the formation of three fused four membered rings, i.e. {ZnSCN}/{ZnSZnS}/{ZnSCN}. The structures resemble the dimeric units found in the *bis*(diethyldithiocarbamates), *bis*(diethyldiselenocarbamates) of zinc, and in mixed alkydialkydithio/selenocarbamates.[28] The Zn-N bonds and Zn-S bond distances and angles are similar to those reported here and in related Zn-dithiocarbamate systems.[28] The S atoms are engaged in both chelating/bridging interactions,

showing significantly longer Zn-S contacts associated with the bridging 3-coordinate S-atoms within the $\{Zn_2S_2\}$ ring [**9**: 2.8149(7) Å; **12**: 2.8061(5) Å] compared to the 2-coordinate S-atoms that participate in only a chelating interaction [**9**: 2.4973(7) Å; **12**: 2.3764(6) Å].

Whilst the zinc centers in each complex are 5 coordinate, the geometry about the zinc atoms in **9** is best described as trigonal bypyramidal ($\tau = 0.70$), and distorted square based pyramidal in the case of **12** ($\tau = 0.36$). These distortions arise as a result of i) the restricted bite distance associated with the chelating ligands [**9**: 62.75(6)° and 62.75(6)° ;**12**: 70.45(5)° and 63.03(5)°], ii) the close approach of the dimer forming S atoms [**9**: 2.3645(7)°; **12**: 2.3666(6)°], and iii) the relative orientation of the *iso*-propyl and mesityl substituents within the two molecules.

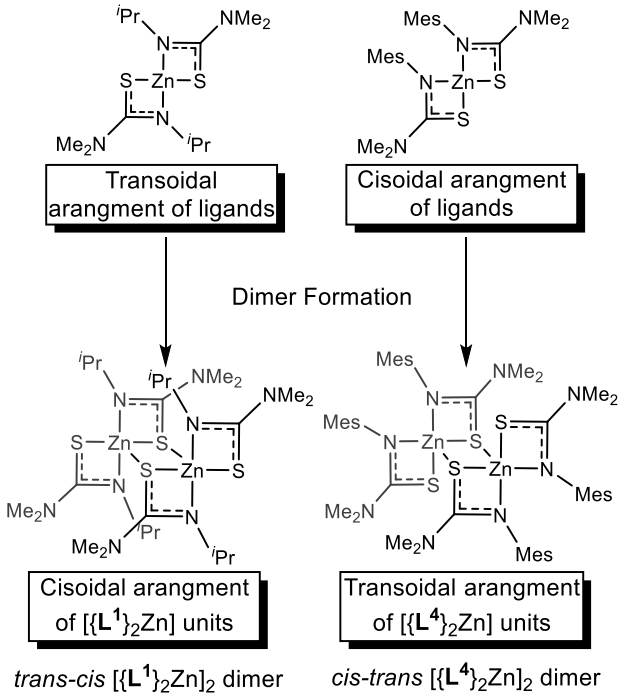

Figure 6: Diagram showing the relative orientation of the {^{i}Pr} and {Mes} substituents in the dimers [{$\mathbf{L^1}$}$_2$Zr]$_2$ (**9**) and [{$\mathbf{L^4}$}$_2$Zr]$_2$ (**12**).

Within each [{$\mathbf{L^1}$}$_2$Zr] unit of complex **9**, the two {^{i}Pr} groups on the chelating thioureide ligands are arranged in *transoidal* fashion, with each [{$\mathbf{L^1}$}$_2$Zr] unit within the dimer then itself arranged *cisoidaly*, resulting in a *trans-cis* [{$\mathbf{L^1}$}$_2$Zr]$_2$ dimer (Figure 6). Contrastingly, in **12**, the two {Mes} groups on the thioureide ligands within each [{$\mathbf{L^4}$}$_2$Zr] unit are arranged in a *cisoidal* fashion about each zinc atom. Each [{$\mathbf{L^4}$}$_2$Zr] unit within the dimer then arranges itself in a *trans* arrangement resulting in a *cis-trans* [{$\mathbf{L^4}$}$_2$Zr]$_2$ dimer (Figure 6). It should be noted that in the case of **12**, the relative displacement of the mesityl groups on the *cis*-[{$\mathbf{L^4}$}$_2$Zr] unit is such that π-π stacking is possible with the closest contact between the two approximately parallel {Mes} rings found to be 3.69(8) Å.

Thermal Profiles: The synthesis of Zn(II) *bis*-thioureide compounds has been driven by our interest in the discovery of novel precursors for the MOCVD of ZnS thin films. As such, thermogravimetric analysis (TGA) was employed to investigate the volatility and thermal stability of complexes **1-12**.

Table 5: Melting point, Onset Temp., % Residual mass and expected %wt for ZnS in complexes **1**, **2**, **4-9** and **12**.

Compound	Onset Temp.‡	% Residual mass (Temp.)	Expected % wt for ZnS.
1	160.2 °C	31.3% (440 °C)	43.5%
2	175.4 °C	33.0% (450 °C)	36.9%
4	225.8 °C	13.5% (450 °C)	32.3%
5	180.2°C	25.9% (360 °C)	26.3%
6	140.0 °C	25.2% (330 °C)	25.3%
7	175.3 °C	21.2% (450 °C)	23.7%
8	225.6 °C	26.0% (475 °C)	21.8%
9	142.1 °C	21.3% (420 °C)	27.4%
12	190.5 °C	18.1% (430 °C)	19.2%

‡ Defined as temperature at 1% mass loss.

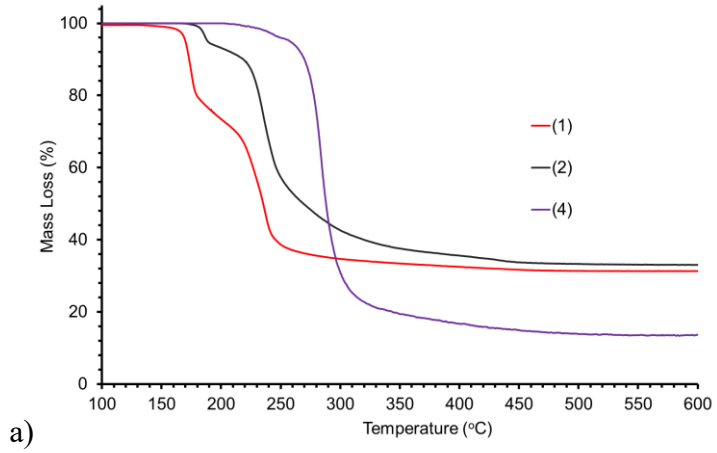

a)

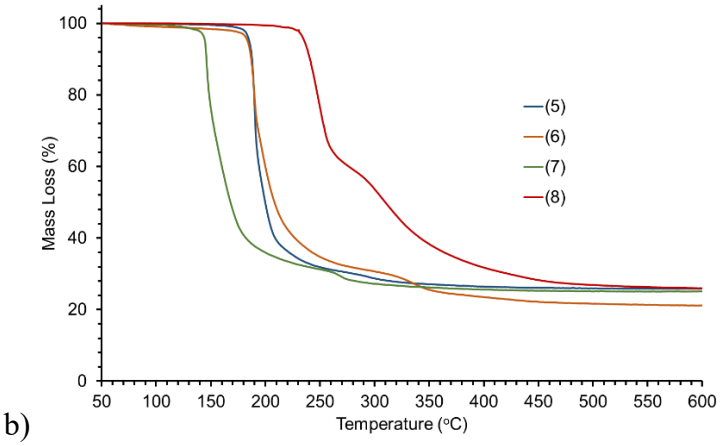

b)

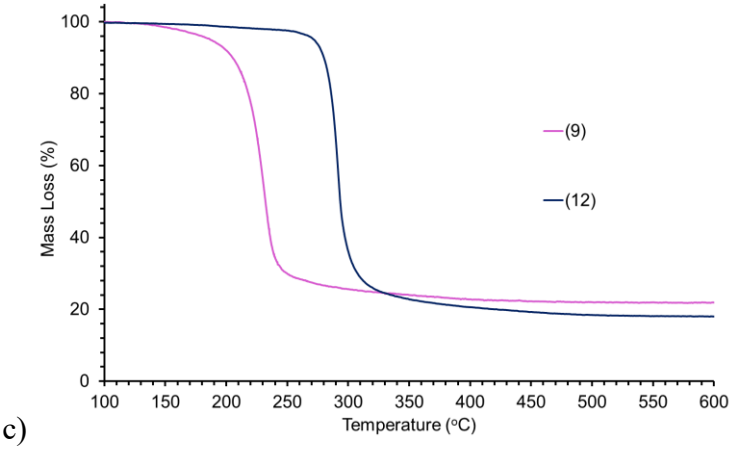

c)

Figure 7: Thermogravimetric plots for complexes **1**, **2** and **4** (a), **5-8** (b) and **9** and **12** (c). (5 °C min^{-1}, 20 ml min^{-1} N_2 flow)

Table 5 shows the onset of mass loss, % mass residues and the expected % mass residue for ZnS from each of the synthesized complexes. Because of its polymeric nature, the Bu^t-derivative (**3**), was not investigated further as a potential ZnS precursor. Similarly, because of the low decomposition temperature of the *bis*-thioureide complexes **10** and **11**, thermogravametric studies were not undertaken.

TG analysis of the methyl zinc thioureide complexes, **1** and **2**, shows multistep decomposition pathways yielding % residues which are both lower than the expected % residue for the formation of ZnS, suggestive of a degree of volatility in the complexes (Figure 7a). In contrast, the mesityl derivative (**4**) shows a higher degree of thermal stability than that observed for **1** (160.2 °C) and **2** (175.4 °C). In contrast to complexes **1** and **2**, the mesityl derivative **4** displays a sharp single step mass loss over a narrow temperature range of (~250 – 330 °C), resulting in a significantly lower % residual mass than that of ZnS or Zn (13.5% *cf.* 32.2%, 21.7% respectively) suggestive of a significantly high degree of volatilization.

For the zinc amide complexes **5**-**8**, the thermal decomposition processes were all found to be multistep, displaying rapid mass loss in the initial phase, tapering off over a wide temperature range (Figure 7b) to reach mass residues which are all close to the expected values for the formation of ZnS, with the exception of the Bu^t derivative (**7**) which is fractionally lower.

For the *bis*-thioureides **9** and **12**, the TGA plots (Figure 7c) clearly display two complexes which, whilst both displaying a single mass loss event, display very different thermal stabilities. For the isopropyl derivative **9**, mass loss begins at ~142 °C, whereas, for the mesityl derivative **12**, mass loss only occurs at ~190 °C (*cf.* 225.6 °C for [{**L**^{4}}ZnMe]$_2$ (**4**) and 225.6 °C for [{**L**^{4}}Zn(N(SiMe$_3$)$_2$)]$_2$ (**8**)). In both instances, the resulting % residual masses (21.3 wt% and 18.1

wt%, respectively) are lower than that expected for the formation of ZnS (27.4 wt% and 19.4 wt%, respectively). In an attempt to ascertain possible decomposition pathways for precursors **9**, TGA-coupled mass spectrometry was undertaken. Unfortunately TGA-MS experiments did not yield conclusive results with respect to precursor decomposition pathways: Peaks at *m/z* = 45 amu and *m/z* = 101.1 amu, were observed in the mass spectra which we attribute to formation of dimethylamine and isopropyl isothiocyanate respectively, suggestive of a de-insertion pathway. We suggest that these results provide strong further support for the generalized assumption that thiouride ligands are potentially significant ligands for the development of stable metal sulfide precursors.

Thin Film Deposition

The low onset temperature for the decomposition of compound **9** (~142 °C), in conjunction with ease of synthesis, stability, and reasonable solubility in THF, led us to assess its viability as a low temperature single source precursor for the AACVD of ZnS thin films. As part of a preliminary viability study, films were deposited under hot wall conditions in a previously described CVD reactor[19, 21-22, 24] onto silica-coated float glass substrates (Pilkington NSG Ltd.). The deposition conditions are shown in Table 6. The films were deposited from 0.15 M solutions of **9** in THF (optimized) onto (100) silicon wafers and glass substrates, at temperatures of 150, 200, 250 and 300 °C for films **A**-**D** respectively.

Table 6: Deposition conditions used for the AACVD of ZnS thin films with compound **9**.

Film	Concentration (mol dm^{-3})	Substrate Temperature (°C)	Deposition Time (min)
A	0.15	150	60
B	0.15	200	60
C	0.15	250	60
D	0.15	300	60

The films (**A**–**D**) were primarily transparent in appearance with more visually yellow material at the leading edge of the substrate, which could indicate the presence of S rich ZnS. At the lower deposition temperatures (150 °C and 200 °C), films **A** and **B** appeared to be very thin and slightly opaque with a very slight yellow appearance. Higher temperatures, however, delivered significantly improved coverage of the substrate to provide films that were transparent.

The films (**A**-**D**) were air and water stable, showing no observable change (as determined by powder X-ray diffraction (PXRD) and UV-Vis transmission spectroscopy) over a period of 2 months. The films were insoluble in common organic solvents but were quickly decomposed in dilute nitric acid and bleach, yielding H_2S.

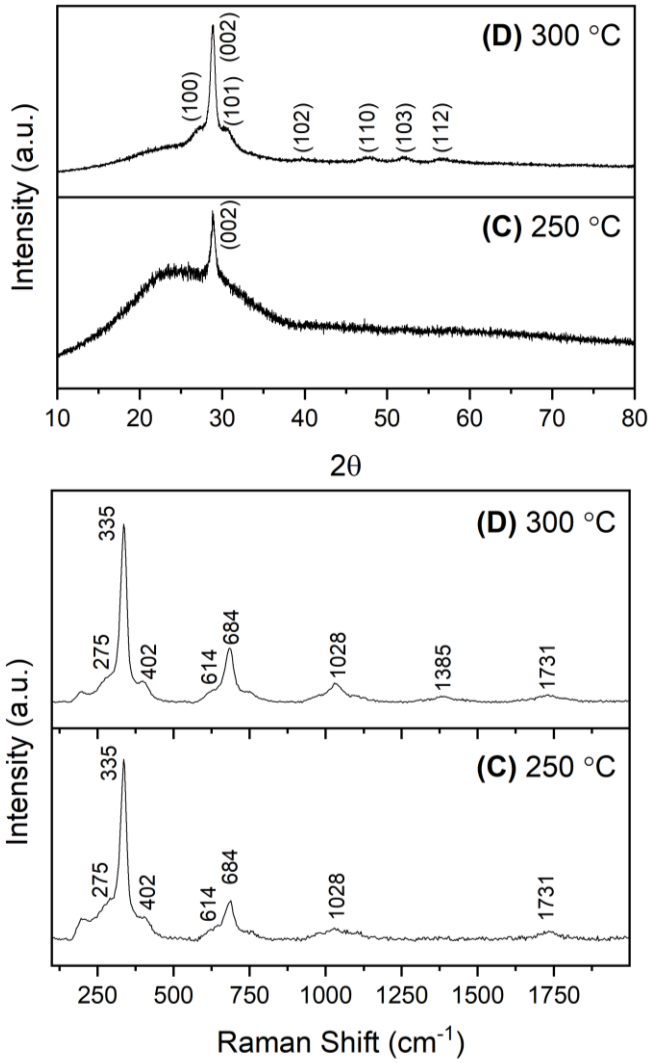

Figure 8: (a) PXRD patterns of films **C**-**D** resulting from AACVD with compound **9**, (b) Raman spectra of films **C**–**D**.

Films **C** and **D**, deposited at 250 and 300 °C respectively, appeared transparent with slight yellowing at the leading edge of the substrate. The mechanical integrity of the as-deposited thin films was assessed using the "Scotch Tape test".[29] The Scotch tape test resulted in no obvious removal of material from the films **C** and **D**, however some material was removed from the surface of films **A** and **B**, suggesting less well adhered films. PXRD analysis was performed on all the deposited films to determine the crystallinity of the materials. Similar analysis of the slightly

yellow regions of the films yielded analogous results. Representative PXRD patterns for the films **C** and **D** are shown in Figure 8.

Films **A** and **B**, deposited at 150 and 200 °C respectively, were found to be amorphous within the limits of the instrument. Films **C** and **D**, deposited at 250 and 300 °C respectively, provided clear indication of crystallinity with one high intensity maximum, which could be readily indexed to the (002) reflection of W-ZnS (JCPDS 36-1450), indicative of ZnS films of polycrystalline nature with a hexagonal close-packed structure. The reflection corresponding to the (002) planes increased in intensity for films deposited at higher temperature. For film **D**, broader peaks also present in the PXRD pattern could be indexed as the (100), (101), (102), (110), (103) and (112) reflections of W-ZnS. For the ZnS films **C** and **D**, PXRD suggests that crystallites are preferentially oriented with (002) planes parallel to the substrate surface, with the *c*-axis of the hexagonal cell normal to the substrate. In order to obtain more structural information, the mean crystallite size (*D*) of the films were calculated using the Debye-Scherrer formula. For films **C** and **D** the minimum domains in the (*00L*) dimension, calculated from X-ray line broadening using the (002) peak, were found to be 9.4 nm and 25.0 nm respectively, such that the films with greater thickness are characterized by greater crystallite size. Experimentally, the 2Θ positions corresponding to the (002) direction changed from 27.9 to 28.8° as the deposition temperature was increased from 250 °C, **C**, to 300 °C, **D**. A simple calculation confirmed that the lattice constants of the c-axes for both films were close to and within experimental error of the reported lattice parameter for W-ZnS (6.402(8) Å).[30]

The Raman spectra of the crystalline films **C** and **D** (Figure 8) displayed absorptions at 275 (TO), 335 (SO), 402 (TA+TO), 614 (2TO) and 684 (2LO) cm^{-1}. These vibrations correspond with

those reported for W-ZnS in the literature.[31] In both the PXRD and Raman spectra, no peaks from any impurities such as ZnO or other compounds are detected.

Deposition temperature, as well as choice of precursor, clearly has a clear effect on the morphology, crystallite size and film thickness of the as deposited thin films. The role of the carrier solvents have also previously been seen to influence the morphology of the films, (*e.g.*, tungsten oxide[32] and tin oxide[33]), and is generally attributed to: Concentration effects; Chemical effects; Modulation of the rates of deposition and droplet evaporation. The latter of these effects is more likely the dominant effect here, for solvents such as toluene and THF, which do not form reactive radical species at the temperatures used in our experiments. Attempts to increase the concentration of precursor, and change the carrier solvent from THF to toluene were met with varying degrees of success. Initial investigations of precursor concentrations >0.15M (in THF) resulted in inconsistent thin film deposition at 300 °C. The reduced solubility of complex **9** in toluene also resulted in uneven film growth from 0.1M solutions of **9** in toluene.

Table 7: Structural Characteristics of ZnS Thin Films.

Film	Roughness Values (nm) †	Film Thickness (*d*) (nm) ‡	Average Crystallite size (*D*) (nm)	Lattice parameter (Å) (c)
A	2.63	53.83	-	-
B	6.54	61.52	-	-
C	7.02	339.88	9.38	6.39 ($2\Theta = 27.9°$)
D	14.59	443.96	24.97	6.19 ($2\Theta = 28.8°$)

†: As determined from AFM over three positions. ‡ As determined by SEM.

Atomic force microscopy (AFM) (ESI) was performed to determine the root-mean-square (rms) surface roughness of the ZnS thin films (Table 7). In all cases, films **A**-**D** were relatively smooth, and were consistent with our observation that with increasing deposition temperature there was an attendant increase in crystallite size, such that films **A** and **B** were significantly less crystalline,

with RMS values of 2.6 nm and 6.5 nm respectively, compared to the more crystalline thin films **C** and **D** (RMS values of 7.0 and 14.6 nm).

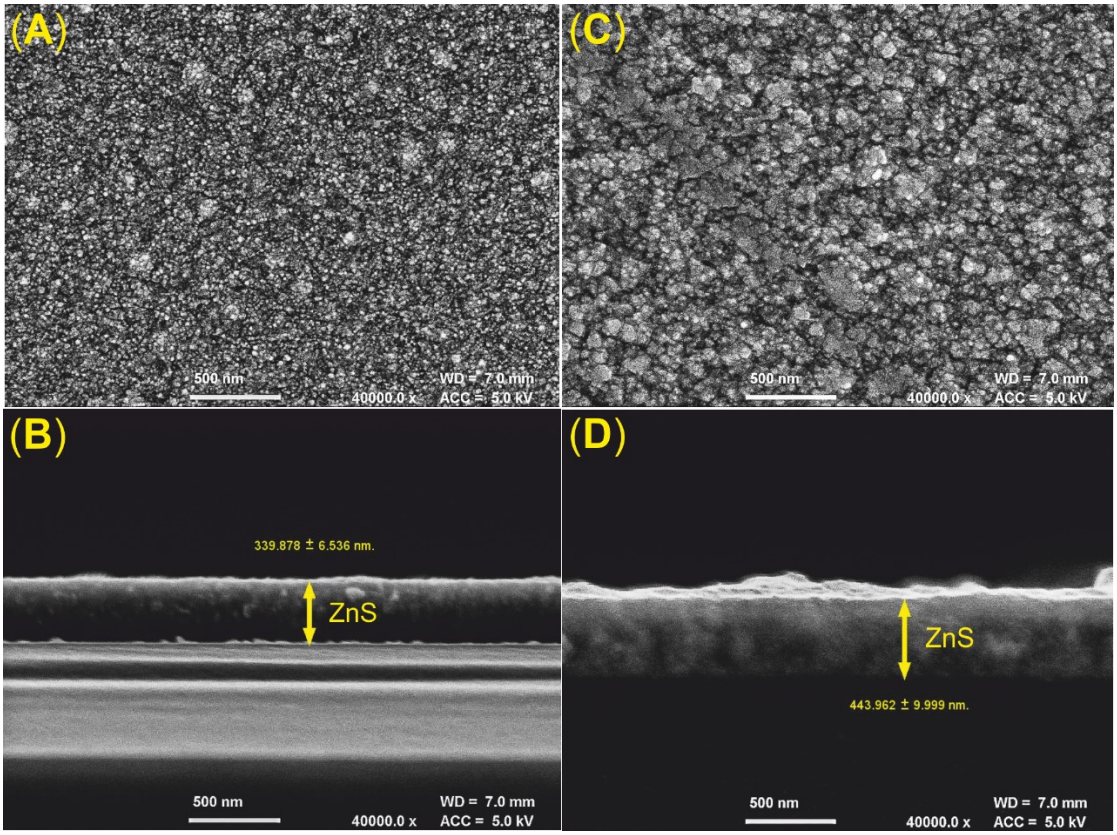

Figure 9: FE-SEM images AACVD ZnS films from compound **9**: (a) plan view of film **C** (250 °C); (b) cross section view of film **C** (250 °C); (c) plan view of film **D** (300 °C); (d) cross section view of film **D** (300 °C).

Figure 9 displays images obtained from field emission scanning electron microscopy (FESEM), which was carried out to determine the morphology of the films. The plan view of films **C** and **D** (Figure 9a & 9c) and the cross-section image (Figure 9b & 9d) both illustrate that the thin films comprise a collection of densely packed crystallites that are globular in appearance. For film **D** these crystallites (Figure 9c) are significantly larger (30-70 nm) than those observed in film **C**

(40-50 nm). This trend is also observed in films **A** and **B**, where crystallite size decreases in line with deposition temperature, and is consistent with the PXRD and AFM data. For films **A** and **B** FE-SEM images are shown in the supplementary information.

Energy dispersive X-ray (EDX) measurements revealed the presence of Zn and S in all thin films deposited. Films deposited at 150 °C (**A**) displayed a relative ratio of Zn:S of 1:1.05, close to the ideal 1:1 ratio, whilst films deposited at higher temperatures, *i.e.* 200 °C (**B**), 250 °C (**C**) and 300 °C (**D**) all appear to be sulfur rich with Zn/S ratios of 1.47, 1.41 and 1.39, respectively, consistent with Zn/S ratios of p-type (S-rich) ZnS.[34] Whilst it is possible that these films could may be more accurately described as co-crystalline ZnS with additional S, there is no evidence of the presence of crystalline or amorphous sulfur from PXRD or Raman spectroscopy analysis.

The room temperature UV–vis absorption spectra of the ZnS samples in the wavelength range 400–850 nm were recorded. All films displayed good visible light transmission, with optical transmission (λ = 400–700 nm) ≥ 75% in all cases. Band gap energies were estimated to lie in the range 3.71 to 3.79 eV from representative Tauc plots (Figure 10). These observations are commensurate with the films behaving as the bulk semiconductor, with direct band gaps similar to those reported elsewhere in the literature for ZnS.[35]

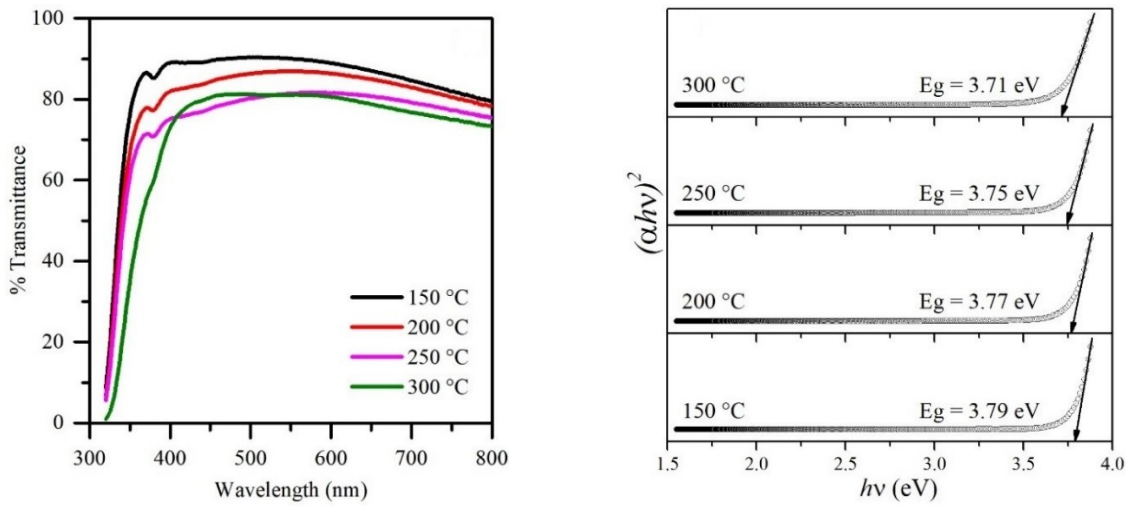

Figure 10: (a)UV-Vis Transmission plots of films **A-D** (150 °C, 200 °C, 250 °C and 300 °C respectively) resulting from AACVD with compound **9**, (b) Tauc plots of films **A**–**D**.

Conclusions

A family of zinc thioureide systems have been described and their potential for the deposition of thin films of ZnS by AACVD has been explored. The homoleptic precursor, $[\{\mathbf{L^1}\}_2Zn]_2$ (**9**) bearing the isopropyl-thiouride ligand was used to deposit ZnS film in the temperature range 150–300 °C, with hexagonal (Wurtzite) W-ZnS deposited at temperatures of 250 °C and above, as identified by PXRD and Raman spectroscopy. EDX analysis confirmed the deposition of ZnS over the entire temperature range with the manifestation of S-rich films at higher temperatures. Optical analysis of the thin films shows high optical transmission and band gap estimations of between 3.17 to 3.79 eV. This study builds on our work, described elsewhere,[22] on the efficacy of thioureide systems as a novel class of precursor for the deposition of metal sulfide thin films. In contrast to our previous study[22] into Sn(II) thioureide systems in which the control of the deposition temperature has a direct effect on the phase of SnS deposited (α or π), no such control is observed here, and no obvious correlation between precursor structure and phase of ZnS deposited can be discerned.

Further work on the structure-reactivity relationships of metal thioureide complexes for the deposition of a range of metal sulfide thin films is ongoing.

Experimental

General Procedures: All reactions were carried out under an inert atmosphere using standard Schlenk techniques. Solvents were dried over activated alumina columns using an Innovative Technology solvent purification system (SPS) and degassed under an argon atmosphere. $Zn(N(SiMe_3)_2)_2$ was produced according to literature procedures,[36] and all other reagents were purchased from commercial sources.

Elemental analyses were performed externally by London Metropolitan University Elemental Analysis Service, UK. ^1H, ^{13}C and ^{119}Sn NMR spectra were recorded on Bruker Advance 300 or 500 MHz FT–NMR spectrometers, as appropriate, in C_6D_6 at room temperature. Chemical shifts are given in ppm with respect to Me_4Si (^1H, ^{13}C). UV-Vis spectra were recorded using a PerkinElmer LAMBDA 750/650 UV/vis/near-IR spectrophotometer. Measurements were recorded at 1400 to 400 nm and zero referenced using 5 mm high-grade Pilkington-NSG float-glass substrates. The measurements were recorded at 1 nm increments.

Synthesis of the pro-ligand [^{i}PrN(H)CSNMe$_2$] (HL^1):

In a dry round bottom flask under nitrogen, dimethylamine was bubbled through a colorless solution of isopropyl isothiocyanate (4.23g, 30mmol) in hexane (100 ml) at 0 °C yielding a white precipitate. The product was extracted from solution by filtration and washed with hexane. Yield 3.69g (84%), (m.p. 75-77°C). ^{1}H NMR (500 MHz, C_6H_6) δ_H: 0.99 (m, 6H (CH*Me*$_2$), 2.52 (s, 6H, N*Me*$_2$), 4.42 (br s, 1H, N(*H*)), 4.87 (m, 1H, C*H*Me$_2$); ^{13}C{^{1}H} NMR (125.7 MHz, C_6D_6) δ_C; 22.9 (CH(*C*H$_3$)$_2$), 39.4 (N*Me*$_2$), 47.3 (*C*H(CH$_3$)$_2$), 182.1 (*C*=S); Elemental analysis (expected): C 49.31% (49.28%); H 9.62%, (9.65%); N 19.18% (19.15%)

Synthesis of the pro-ligands [CyN(H)CSNMe$_2$] (HL^2), [^{t}BuN(H)CSNMe$_2$] (HL^3) and [MesN(H)CSNMe$_2$] (HL^4).

The pro-ligands H**L^2**-H**L^4** were made in an analogous manner to H**L^1** using of 5.59g (30mmol) cyclohexyl isothiocyanate, 4.81g (30mmol) of tertiary-butyl isothiocyanate and 5.32g (30 mmol) of 2,4,6-trimethylphenyl isothiocyanate, respectively.

HL^2: Yield: 4.81g (86%) (m.p. 91-93°C). ^{1}H NMR (500 MHz, C_6D_6): δ_H 0.85-1.06 (m, 3H, C*H*$_2$), 1.20-1.32 (m, 2H, C*H*$_2$), 1.42-1.48 (m, 1H, C*H*$_2$), 1.49-1.57 (m, 2H, 6H, C*H*$_2$), 2.08-2.15 (m, 2H, C*H*$_2$), 2.63(br s, 6H, N*Me*$_2$), 4.64 (br m, 1H, NC(*H*)) 4.73 (br S, 1H, N(*H*)); ^{13}C{^{1}H} NMR (125.7 MHz, C_6D_6); δ_C 25.4 (*C*H$_2$), 26.1 (*C*H$_2$), 33.5 (*C*H$_2$), 39.5 (*C*H$_3$), 54.3 (*C*H), 181.9 (*C*=S); Elemental analysis (expected): C 58.02% (58.02%), H 9.78% (9.74%), N 15.08% (15.04%).

HL^3: Yield: 3.89g (81%) (m.p. 57-58°C). ^{1}H NMR (500 MHz, C_6D_6) δ_H 1.51 (s, 9H, C*Me*$_3$), 2.60, (s, 6H, N*Me*$_2$), 4.72 (bs s, 1H, N(*H*)); ^{13}C{^{1}H} NMR (125.7 MHz, C_6D_6) δ_C 29.3 (C*Me*$_3$), 39.6 (N*Me*$_2$), 53.7 (*C*Me$_3$), 181.7 (*C*=S); Elemental analysis (expected): C 52.59% (52.46%), H 10.09% (10.06%), N 17.51% (17.48%).

HL^4: Yield: 5.47g (82%); (177-180°C) ^{1}H NMR (500 MHz, C_6D_6) δ_H 2.17 (s, 3H, *para*-C*H*$_3$), 2.20 (s, 6H, *ortho*-C*H*$_3$), 2.64 (s, 6H N*Me*$_2$), 5.64 (br s, 1H, N(*H*)), 6.82 (s, 2H, Ar-C*H*); ^{13}C{^{1}H} NMR (125.7 MHz, C_6D_6) δ_C; 18.6 (*ortho*-*C*H$_3$) 21.1 (*para*-CH), 40.2 (N*Me*$_2$), 129.2 (Ar-*C*H), 135.7 (Ar-*C*), 136.5 (Ar-*C*), 136.7 (Ar-*C*), 183.0 (*C*=S); Elemental analysis (expected): C 64.82% (64.83%), H 8.16% (8.16%), N 12.60% (12.58%).

Synthesis of [{^{i}PrNC(S)NMe$_2$}ZnMe]$_2$ ([{L^1}ZnMe]$_2$) (1)

To a cooled solution of H**L^1** (0.197g, 1.35 mmol) in 20ml of toluene was added 0.675ml (1.35mmol) of a 2.0 M dimethyl zinc solution in toluene and the resulting reaction mixture left to stir overnight. Visible gas was seen to be produced in the colorless solution. The solution was reduced *in vacuo*, and recrystallized at -28 °C affording white crystals. Yield: 0.13 g (43%). ^{1}H NMR (500 MHz, C_6D_6): δ_H -0.01 (s, 3H, Zn-C*H*$_3$), 1.03 (d, J = 6.20Hz, 6H, -NCH*Me*$_2$), 2.58 (s, 6H, -N*Me*$_2$, 3.50 (sept, J = 6.20 Hz, 1H, -NC*H*Me$_2$); ^{13}C{^{1}H} NMR (125.7 MHz, C_6D_6): δ_c -11.9 (Zn-*Me*), 25.0 (NCH*Me*$_2$), 42.9 (-CN*Me*$_2$), 49.8 (N*C*HMe$_2$), 173.0 (S-C-NMe$_2$); Elemental analysis for $C_{14}H_{32}N_4S_2Zn_2$ (expected): C 37.19% (37.26%), H 7.17% (7.15%), N 12.39% (12.41%).

Synthesis of [{CyNC(S)NMe$_2$}ZnMe]$_2$ ([{L^2}ZnMe]$_2$) (2), [{^{t}BuNC(S)NMe$_2$}ZnMe]$_\infty$ ([{L^3}ZnMe]$_\infty$) (3) and [{MesNC(S)NMe$_2$}ZnMe]$_2$ ([{L^4}ZnMe]$_2$) (4).

The complexes **2-4** were made in an analogous manner to **1** using of 0.186g, (1 mmol) of H**L^2**, 0.139g (1 mmol) of H**L^3** and 0.22g (1 mmol) of H**L^4** respectively.

2: Yield: 0.08 g (29%). ^{1}H NMR (500 MHz, C_6D_6): δ_H 0.05 (s, 3H, Zn-*Me*), 1.08-0.91 (m, 2H, Cy-C*H*$_2$), 1.46-1.35 (m, 2H, Cy-C*H*$_2$), 1.60-1.49 (m, 2H, Cy-C*H*$_2$), 1.87-1.75 (m, 2H, Cy-C*H*$_2$),

2.63 (s, 6H, -N*Me*$_2$), 3.25-3.19 (br m, 1H, -NC*H*(Cy)); $^{13}C\{^1H\}$ NMR (125.7 MHz, C_6D_6): δ_C -11.8 (Zn-*Me*), 25.6 (Cy-*C*H$_2$), 25.8 (Cy-*C*H$_2$), 36.0 (Cy-*C*H$_2$), 43.0 (-N*Me*$_2$), 58.5 (-N*C*HCy), 173.0 (S-*C*-NMe$_2$); Elemental analysis for $C_{20}H_{40}N_4S_2Zn_2$ (expected): C 45.18% (45.20%), H 7.58% (7.59%), N 10.54% (10.54%).

3: Yield: 0.22 g (93%). ^1H NMR (500 MHz, C_6D_6): δ_H 0.01 (s, 3H, Zn-*Me*), 1.22 (s, 9H, -NC*Me*$_3$), 2.47 (s, 6H, -N*Me*$_2$); $^{13}C\{^1H\}$ NMR (125.7 MHz, C_6D_6) δ_C -11.5 (Zn-*Me*), 31.0 (-N*C*Me$_3$), 44.4 (-NMe$_2$), 55.4 (-N*C*Me$_3$), 181.9 (S-*C*-NMe$_2$); Elemental analysis for $C_{16}H_{36}N_4S_2Zn_2$ (expected): C 39.98% (40.09%), H 7.60% (7.57%), N 11.68%, (11.69%).

4: Yield: 0.31 g, (99%); ^1H NMR (500 MHz, C_6D_6): δ_H 0.41 (br s, 3H, Zn-*Me*), 2.06 (s, 6H, *ortho*-*Me*), 2.15 (s, 3H, *para*-*Me*), 2.42 (s, 6H, -N*Me*$_2$), 6.61 (s, 2H, Ar-C*H*); $^{13}C\{^1H\}$ NMR (125.7 MHz, C_6D_6): δ_C -10.4 (Zn-*Me*), 19.0 (*ortho*-*Me*), 20.9 (*para*-*Me*), 42.0 (-N*Me*$_2$), 131.8 (*ortho*-*C*Me), 132.4 (*para*-C*Me*), 144.2 (-N-C), 178.0 (S-*C*-NMe$_2$); Elemental analysis for $C_{26}H_{40}N_4S_2Zn_2$ (expected): C 51.69%, (51.74%), H 6.65% (6.68%), N 9.28% (9.28%).

Synthesis of [{^{i}PrNC(S)NMe$_2$}Zn{N(SiMe$_3$)$_2$}]$_2$ ([{L^1}Zn{N(SiMe$_3$)$_2$}]$_2$) (5)

A cooled solution of Zn{N(SiMe$_3$)$_2$}$_2$ (0.39g, 1mmol) dissolved in toluene, was combined with a solution of the pro ligand H**L^1** (0.146g, 1 mmol) in toluene (20 ml), and allowed to stir for 8h. *In vacuo* removal of solvent resulted in the formation of a cloudy suspension, which was resolved which gentle heating, and allowed to crystallize at -28 °C affording white crystals. Yield: 0.25 g (67%). ^1H NMR (500 MHz, C_6D_6) δ_H 0.46 (s, 18H, Zn-N(Si*Me*$_3$)$_2$) 1.20-1.13 (m, 6H, -NCH*Me*$_2$), 2.63 (s, 6H, -N*Me*$_2$), 3.62-3.53 (m, 1H, -NC*H*Me$_2$); $^{13}C\{^1H\}$ NMR (125.7 MHz, C_6D_6): δ_C 6.4 (Zn-N(Si*Me*$_3$)$_2$), 24.9 (-NCH*Me*$_2$), 43.6 (-N*Me*$_2$), 50.9 (-N*C*HMe$_2$), 186.1 (S-C-NMe$_2$); Elemental

analysis for $C_{24}H_{62}N_6S_2Si_4Zn_2$ (expected): C 38.37% (38.85%), H 8.38%, (8.42%), N 11.35% (11.33%).

Synthesis of [{CyNC(S)NMe$_2$}Zn{N(SiMe$_3$)$_2$}]$_2$ ([{L^2}ZnN{N(SiMe$_3$)$_2$}]$_2$) (6), [{^{t}BuNC(S)NMe$_2$}ZnN{N(SiMe$_3$)$_2$}]$_2$ ([{L^3}ZnN{N(SiMe$_3$)$_2$}]$_2$) (7) and [{MesNC(S)NMe$_2$}ZnN{N(SiMe$_3$)$_2$}]$_2$ ([{L^4}ZnN{N(SiMe$_3$)$_2$}]$_2$) (8).

The complexes **6-8** were made in an analogous manner to **5** using of 0.186g, (1 mmol) of H**L^2**, 0.139g (1 mmol) of H**L^3** and 0.22g (1 mmol) of H**L^4** respectively.

6: Yield: 0.29 g (70%). ^{1}H NMR (500 MHz, C_6D_6) δ_H 0.48 (s, 3H, Zn-N(Si(*Me*$_3$)$_2$), 1.13-1.03 (m, 2H, Cy-C*H*$_2$), 1.51-1.45 (m, 2H, Cy -C*H*$_2$, 1.70-1.60 (m, 2H, Cy-C*H*$_2$), 1.91-1.815 (m, 2H, Cy-C*H*$_2$), 2.67 (s, 6H, -N*Me*$_2$), 3.33-3.22 (m, 1H, -NC*H*Cy); ^{13}C{^{1}H} NMR (125.7 MHz, C_6D_6) δ_C 6.7 (Zn-N(Si*Me*$_3$), 25.6 (Cy-*C*H$_2$), 25.7 (Cy-*C*H$_2$), 35.9 (Cy-*C*H$_2$), 43.6 (-N*Me*$_2$), 59.0 (-N*C*HCy), 179.2 (S-*C*-NMe$_2$); Elemental analysis for $C_{30}H_{70}N_6S_2Si_4Zn_2$ (expected): C 43.86%, (43.83%), H 8.53% (8.58%), N 10.32% (10.22%).

7: Yield: 0.16 g (42%); ^{1}H NMR (500 MHz, C_6D_6): δ_H 0.44 (s, 18H, Zn-N(Si*Me*$_3$)$_2$), 1.31 (s, 9H, -NCMe$_3$), 2.52 (s, 6H, -N(C*H*$_3$)$_2$); ^{13}C{^{1}H} NMR (125.7 MHz, C_6D_6): δ_C 6.6 (Zn-N(Si*Me*$_3$), 31.1 (-NC*Me*$_3$), 44.7 (-N*Me*$_2$), 57.9 (-N*C*Me$_3$), 179.1 (S-*C*-NMe$_2$); Elemental analysis for $C_{26}H_{66}N_6S_2Si_4Zn_2$ (expected): C 39.96%, (40.55%), H 8.69% (8.64%), N 10.98% (10.91%).

8: Yield: 0.23 g (52%); ^{1}H NMR (500 MHz, C_6D_6) δ_H 0.31 (s, 18H, -N(Si*Me*$_3$)$_2$), 2.09 (s, 3H, *para*-*Me*), 2.35 (s, 6H, *ortho*-*Me*), 2.58 (s, 6H, -N*Me*$_2$), 6.73 (s, 2H, *meta*-C*H*); ^{13}C{^{1}H} NMR (125.7 MHz, C_6D_6) δ_C 6.0 (-N(SiMe$_3$)$_2$), 19.4 (*ortho*-*Me*), 20.9 (*para*-*Me*), 42.9 (-N*Me*$_2$), 128.9 (*meta*-*C*H), 134.2 (*para*-*C*-Me), 143.5 (*ortho*-*C*-Me), 144.3 (-N-*C*), 168.4 (S-*C*-NMe$_2$); Elemental

analysis for $C_{36}H_{70}N_6S_2Si_4Zn_2$ (expected): C 48.87%, (48.83%), H 7.86% (7.89%), N 9.57% (9.40%).

Synthesis of *Bis*-[{^{i}PrNC(S)NMe$_2$}$_2$Zn]$_2$ ([{L^1}$_2$Zn]$_2$) (9)

Zn{N(SiMe$_3$)$_2$}$_2$ (0.39g, 1mmol) was dissolved in toluene (20ml) and added to a cooled solution of the pro-ligand H**L^1** (0.292g, 2 mmol) in 20ml of toluene, and stirred for 8h. The volume of solvent was reduced by half, *in vacuo*, yielding a cloudy suspension which was redissolved with gentle heating, and allowed to crystallize at -28 °C, affording white crystals. Yield; 0.21g (60%). ^{1}H NMR (300 MHz, C_6D_6) δ_H 1.21 (m, 6H, -NCH*Me*$_2$), 2.64 (s, 6H, -NMe$_2$), 3.63 (m, 1H, -NC*H*Me$_2$); ^{13}C{^{1}H} NMR (75.5 MHz, C_6D_6) δ_C 25. 8 (-NCH*Me*$_2$), 43.98 (-N*Me*$_2$), 50.9 (-N*C*H(CH$_3$)$_2$), 181.0 (S-*C*-NMe$_2$); Elemental analysis for $C_{24}H_{52}N_8S_4Zn_2$:C_7H_8 (expected): C 46.33%, (46.32%), H 7.50% (7.52%), N 14.13% (13.94%).

Synthesis of *Bis*-[{CyNC(S)NMe$_2$}$_2$Zn] ([{L^2}$_2$Zn]) (10), *Bis*-[{^{t}BuNC(S)NMe$_2$}$_2$Zn]$_2$ ([{L^3}$_2$Zn]$_2$) (11) and *Bis*-[{MesNC(S)NMe$_2$}$_2$Zn]$_2$ ([{L^4}$_2$Zn]$_2$) (12).

The complexes **10-12** were made in an analogous manner to **9** using of 0.186g, (1 mmol) of H**L^2**, 0.139g (1 mmol) of H**L^3** and 0.22g (1 mmol) of H**L^4** respectively.

10: Yield 0.25g (56%); ^{1}H NMR (500 MHz, C_6D_6) δ_H 1.17-1.03 (m, 3H, Cy-C*H*$_2$) 1.51-1.41 (m, 1H, Cy-C*H*$_2$), 1.71-1.57 (m, 2H, Cy -C*H*$_2$), 2.16-1.02 (m, 2H, Cy-C*H*$_2$), 2.65 (s, 6H, -N*Me*$_2$), 3.35-3.23 (m, 1H, -N-C*H*(Cy)); ^{13}C{^{1}H} NMR (125.7 MHz, C_6D_6) δ_C 25.8 (Cy-*C*H$_2$), 36.1 (Cy-*C*H$_2$), 43.4 (-N*Me*$_2$), 58.3 (-N*C*), 181.5 (S-*C*-NMe$_2$); Elemental analysis for $C_{36}H_{68}N_8S_4Zn_2$ (expected): C 49.49% (49.59%), H 8.01% (7.86%), N 12.79% (12.85%).

11: Yield 0.32g (83%); ^{1}H NMR (500 MHz, C_6D_6) δ_H 1.22 (s, 9H, -NC*Me*$_3$), 2.47 (s, 6H, -N*Me*$_2$); ^{13}C{^{1}H} NMR (125.7 MHz, C_6D_6) δ_C 31.0 (-NC*Me*$_3$), 44.4, (-N*Me*$_2$), 65.3 (-N*C*Me$_3$), 182.0 (S-*C*-NMe$_2$); Elemental analysis for $C_{28}H_{60}N_8S_4Zn_2$ (expected): C 43.48% (43.80%), H 7.86% (7.88%), N 14.57% (14.59%).

12: 0.41g, (80%) ^{1}H NMR (500 MHz, C_6D_6) δ_H 2.06 (s, 6H, *ortho*-*Me*), 2.16 (s, 3H, (*para*-*Me*), 2.42 (s, 6H, -N*Me*$_2$), 6.65 (s, 2H, Ar-C*H*); ^{13}C{^{1}H} NMR (125.7 MHz, C_6D_6) δ_C 19.0 (*ortho*-*Me*), 20.9 (*para*-*Me*), 42.0 (-N*Me*$_2$), 110.4 (*ortho*-*C*Me), 128.5 (Ar-*C*H), 132.1 (*para*-C-Me), 144.2 (-N*C*(Ar)), 177.6 (S-*C*-NMe$_2$); Elemental analysis for $C_{48}H_{68}N_8S_4Zn_2$ (expected): C 56.71% (56.74%), H 6.86%, (6.75%), N 10.87% (11.03%).

Single Crystal X-ray Diffraction Studies: Experimental details relating to the single-crystal X-ray crystallographic studies for compounds **1-9** and **12** are summarised in Table S1 (ESI). Single Crystal X-ray crystallography data were collected at 150 K on RIGAKU SuperNova Dual wavelength diffractometer equipped with an Oxford Cryostream, featuring a micro source with MoKα radiation (λ= 0.71073 Å) and CuKα radiation (λ= 1.5418 Å). Crystals were isolated from an argon filled Schlenk flask and immersed under oil before being mounted onto the diffractometer. Structures were solved by direct methods throughout and refined on F^2 data using the SHELXL-2014 suite of programs. All hydrogen atoms were included in idealised positions and refined using the riding model. Refinements were straightforward with no additional points that merit note. CCDC 1881545-1881554 contains the supplementary crystallographic data for this paper. These data can be obtained free of charge at www.ccdc.cam.ac.uk/conts/retrieving.html [or from the Cambridge Crystallographic Data Centre, 12, Union Road, Cambridge CB2 1EZ, UK; fax: +44-1223/336-033; E-mail: deposit@ccdc.cam.ac.uk].

AACVD Experiments

Thin films were deposited using a horizontal hot wall reactor. The aerosol was generated with a TSI 3076 Constant Output Atomiser using N_2 at 20 psi to generate the aerosol and act as the carrier gas. Films were grown on either 2.5 cm × 15 cm SiO_2-coated glass (Pilkington NSG Ltd.), which were cleaned with isopropanol, water, and acetone and then dried under a flow of nitrogen gas, or commercial crystalline silicon. For each deposition a 0.15 M THF solution of **9** was made up in a glovebox, and transferred into a bubbler under an inert atmosphere. Depositions were carried out at 200, 250, 300 and 350 °C for 1 h using N_2 as a carrier gas.

The precursor solution was prepared within a glove box under an atmosphere of argon and all solvents were dried and degassed prior to use. The precursor bubbler was kept under an atmosphere of argon, sealed and attached onto to the AACVD apparatus. Once all substrates were prepared and mounted into the deposition chamber, nitrogen gas was allowed to flow through the system, bypassing the precursor holder, for 20 minutes in order to purge the system with nitrogen. Then with continuing gas flow the hot-wall furnace is switched on and allowed to reach the target deposition temperature and equilibrate for 20 minutes. Once this is achieved the gas flow is diverted to flow via the precursor solution which draws the solution into the TSI 3076 Constant Output Atomiser and out into the deposition chamber where the deposition commences and the timer is started. Gas flow is monitored via bubbler and gas pressure fixed 10 bar until it reaches the atomiser, as described previously.[19, 21-22, 24]

Thermogravimetric Analysis (TGA): TGA was collected using a TGA 4000 Perkin Elmer system. Samples were prepared air sensitively using a crimped aluminium sample pan. TGA was performed under a flow of N_2 at 20 ml min^{-1} and heated from 30 ºC to 600 ºC at a ramp rate of 5 ºC min^{-1}. TGA-MS was performed under argon (20 ml/min) at a ramp rate of 5 °C/min between 30 and 600 °C on a Setaram Setsys Evolution TGA 16/18 with the evolved gases passing through a Pfeiffer Vacuum Omnistar GSD 320 quadrapole mass spectrometer. Samples were contained in alumina crucibles. Experiments were performed by MC^2, University of Bath, UK, and results were analysed using Excel.

Powder X-ray Diffractometry (PXRD): PXRD data was collected on a BRUKER D8-Advance. The X-ray diffraction spectra were collected for the thin films using the flat plate mode from 5 to 70 2θ at 2º per minute. X-rays were generated from a Cu source at wave lengths of 1.54 Å.

Scanning Electron Microscopy (SEM): SEM was performed to visualise the morphology of the films both as cross sections (using a Field Emission Scanning Electron Microscope 6301F) and top down (JEOL 6480 Low Vacuum large stage SEM platform) images. The films were prepared by mounting onto steel SEM mounts with conductive carbon tape attached to the bottom and top surface of the films, to maximise conductivity of electrons and prevent charge accumulation. Samples were desiccated at 35 ºC for 24 hour prior to analysis.

Atomic Force Microscopy (AFM): AFM analysis was performed using a Digital Instruments Nanoscope IIIa, with BRUKER SNL-10 Silicon on Nitride Lever contact tips (tip radius <10 nm,

f_0: 50-80 kHz, k: 0.350 N/m and T: 600nm), in contact mode. Images processed using the open access Gwyddion SPM data analyser.

Energy dispersive X-ray spectroscopy (EDS): EDS was performed using Oxford Instruments Scanning Electron Microscope 6480 LV and processed on INCA Wave software. All spectra were standardised and calibrated against a standard silicon wafer sample. The magnification, working distance and beam energy (10 keV) were kept consistent between spectral analyses.

Raman Spectroscopy: Raman spectra were collected using a Renishaw inVia Raman Microscope fitted with a 532 nm laser at a 10 % spot size, 3 s exposure time and 1 % energy intensity. The data was processed using a Renishaw WiRE software package.

Associated Content

Supporting Information Available: (Figures showing the molecular structures of complexes **5**, **6** and **8**. Experimental details relating to the single-crystal X-ray crystallographic studies and crystallographic data for complexes **1**-**9** and **12**. Additional FE-SEM and AFM images of thin films (PDF).) This material is available free of charge via the Internet at http://pubs.acs.org.

Accession Codes

CCDC **1881545-188154** contain the supplementary crystallographic data for this paper. These data can be obtained free of charge via www.ccdc.cam.ac.uk/data_request/cif, or by emailing

data_request@ccdc.cam.ac.uk, or by contacting The Cambridge Crystallographic Data Centre, 12 Union Road, Cambridge CB2 1EZ, UK; fax: +44 1223 336033.

ACKNOWLEDGMENTS

The authors thank the EPSRC for funding (EP/L016354/1), the Doctoral Training Center in Sustainable Chemical Technologies for a PhD studentship (H.S.I.S.), the University of Bath for financial support (PhD studentship to J. D. P.) and the Royal Thai Government for a postgraduate scholarship (P.T.).

AUTHOR INFORMATION

Corresponding Authors

***E-mail: a.l.johnson@bath.ac.uk**

ORCID

Andrew Johnson: 0000-0001-5241-0878

Author Contributions

The manuscript was written through contributions of all authors. All authors have given approval to the final version of the manuscript.

REFERENCES

(1) (a) Yanagiya, S.-i.; Iseki, Y.; Kaito, T.; Mori, A.; Kaito, C.; Sekiguchi, T.; Inoue, T. Growth of ZnS Nano-Crystallites in Gel and their Characterization. *Mater. Chem. Phys.,* **2007**, *105*, 250-252; (b) Fang, X.; Bando, Y.; Gautam, U. K.; Zhai, T.; Zeng, H.; Xu, X.; Liao, M.; Golberg, D. ZnO and ZnS Nanostructures: Ultraviolet-Light Emitters, Lasers, and Sensors. *Crit. Rev. Solid State .Mater. Sci.,* **2009**, *34*, 190-223; (c) Fang, X.; Zhai, T.; Gautam, U. K.; Li, L.; Wu, L.; Bando, Y.; Golberg, D. ZnS Nanostructures: From Synthesis to Applications. *Prog. Mater. Sci.,* **2011**, *56*, 175-287; (d) Ehsan, M. A.; Peiris, T. A. N.; Wijayantha, K. G. U.; Khaledi, H.; Ming, H. N.; Misran, M.; Arifin, Z.; Mazhar, M. Surface Morphological and Photoelectrochemical Studies of ZnS Thin Films Developed from Single Source Precursors by Aerosol Assisted Chemical Vapour Deposition. *Thin Solid Films,* **2013**, *540*, 1-9

(2) Yeh, C.-Y.; Lu, Z. W.; Froyen, S.; Zunger, A. Zinc-Blende–Wurtzite Polytypism in Semiconductors. *Phys. Rev. B: Condens. Matter.,* **1992**, *46*, 10086-10097

(3) La Porta, F. A.; Gracia, L.; Andrés, J.; Sambrano, J. R.; Varela, J. A.; Longo, E.; Zhou, Y. A DFT Study of Structural and Electronic Properties of ZnS Polymorphs and its Pressure-Induced Phase Transitions. *J. Am. Ceram. Soc.,* **2014**, *97*, 4011-4018

(4) (a) Brafman, O.; Mitra, S. S. Raman Effect in Wurtzite- and Zinc-Blende-Type ZnS Single Crystals. *Phys. Rev.,* **1968**, *171*, 931-934 ; (b) Wagner, H. P.; Kühnelt, M.; Langbein, W.; Hvam, J. M. Dispersion of the Second-Order Nonlinear Susceptibility in ZnTe, ZnSe, and ZnS. *Phys, Rev, B: Condens. Matter.,* **1998**, *58*, 10494-10501; (c) Ding, Y.; Wang, X. D.; Wang, Z. L. Phase Controlled Synthesis of ZnS Nanobelts: Zinc Blende vs Wurtzite. *Chem. Phys. Lett.,* **2004**, *398*, 32-36

(5) (a) Shao, L. X.; Chang, K. H.; Hwang, H. L. Zinc Sulfide Thin Films Deposited by RF Reactive Sputtering for Photovoltaic Applications. *Appl. Surf. Sci.,* **2003**, *212*, 305-310; (b)Subbaiah, Y. P. V.; Prathap, P.; Reddy, K. T. R. Structural, Electrical and Optical Properties of ZnS Films Deposited by Close-Spaced Evaporation. *App. Surf. Sci.,* **2006**, *253*, 2409-2415; (c) Goudarzi, A.; Aval, G. M.; Sahraei, R.; Ahmadpoor, H. Ammonia-Free Chemical Bath Deposition of Nanocrystalline ZnS Thin Film Buffer Layer for Solar Cells. *Thin Solid Films,* **2008**, *516*, 4953-4957

(6) (a) Mandal, S. K.; Chaudhuri, S.; Pal, A. K. Optical Properties of Nanocrystalline ZnS Films Prepared by High Pressure Magnetron Sputtering. *Thin Solid Films,* **1999**, *350*, 209-213; (b) Wei, M.; Choy, K. L. Deposition of Highly Oriented ZnS Thin Films on Si(100) Substrate Using Electrostatic Spray Assisted Vapor Deposition. *Chem. Vap. Deposition,* **2002**, *8*, 15-17; (c) Hernández-Fenollosa, M. A.; López, M. C.; Donderis, V.; González, M.; Marí, B.; Ramos-Barrado, J. R. Role of Precursors on Morphology and Optical Properties of ZnS Thin Films Prepared by Chemical Spray Pyrolysis. *Thin Solid Films,* **2008**, *516*, 1622-1625; (d) Chelvanathan, P.; Yusoff, Y.; Haque, F.; Akhtaruzzaman, M.; Alam, M. M.; Alothman, Z. A.; Rashid, M. J.; Sopian, K.; Amin, N. Growth and Characterization of RF-Sputtered ZnS Thin Film Deposited at Various Substrate Temperatures for Photovoltaic Application. *Appl. Surf. Sci.,* **2015**, *334*, 138-144; (e) Le Donne, A.; Cavalcoli, D.; Mereu, R. A.; Perani, M.; Pagani, L.; Acciarri, M.; Binetti, S. Study of the Physical Properties of ZnS Thin Films Deposited by RF Sputtering. *Mater. Sci. Semicond. Process.,* **2017**, *71*, 7-11

(7) (a) Frigo, D. M.; Khan, O. F. Z.; O'Brien, P. Growth of Epitaxial and Highly Oriented Thin Films of Cadmium and Cadmium Zinc Sulfide by Low-Pressure Metalorganic Chemical Vapour Deposition Using Diethyldithiocarbamates. *J. Cryst. Growth,* **1989**, *96*, 989-992; (b) Hursthouse,

M. B.; Malik, M. A.; Motevalli, M.; O'Brien, P. Mixed Alkyl Dialkylthiocarbamates of Zinc and Cadmium: Potential Precursors for II/VI Materials. X-ray Crystal Structure of $[MeZnS_2CNEt_2]_2$. *Organometallics,* **1991**, *10*, 730-732; (c) Seo, K. W.; Yoon, S. H.; Lee, S. S.; Shim, I. W. Preparation of ZnS Thin Film Using Zn(dithiocarbamate)$_2$ Precursors by MOCVD Method. *Bull. Korean Chem. Soc.,* **2005**, *26*, 1582-1584; (d) Nyamen, L. D.; Nejo, A. A.; Pullabhotla, V. S. R.; Ndifon, P. T.; Malik, M. A.; Akhtar, J.; O'Brien, P.; Revaprasadu, N. The Syntheses and Structures of Zn(II) Heterocyclic Piperidine and Tetrahydroquinoline Dithiocarbamates and Their use as Single Source Precursors for ZnS Nanoparticles. *Polyhedron,* **2014**, *67*, 129-135

(8) (a) Barreca, D.; Tondello, E.; Lydon, D.; Spalding, T. R.; Fabrizio, M. Single-Source Chemical Vapor Deposition of Zinc Sulfide-Based Thin Films from Zinc bis(O-ethylxanthate). *Chem. Vap. Deposition,* **2003**, *9*, 93-98; (b) Barreca, D.; Gasparotto, A.; Maragno, C.; Tondello, E.; Sada, C. CVD of Nanophasic (Zn, Cd)S Thin Films: From Multi-Layers to Solid Solutions. *Chem. Vap. Deposition,* **2004**, *10*, 229-236; (c) Barreca, D.; Gasparotto, A.; Maragno, C.; Seraglia, R.; Tondello, E.; Venzo, A.; Krishnan, V.; Bertagnolli, H. Synthesis and Characterization of Zinc Bis(O-isopropylxanthate) as a Single-Source Chemical Vapor Deposition Precursor for ZnS. *Appl. Organomet. Chem.,* **2005**, *19*, 1002-1009

(9) Pawar, A. S.; Mlowe, S.; Garje, S. S.; Akerman, M. P.; Revaprasadu, N. Zinc Thiosemicarbazone Complexes: Single Source Precursors for Alkylamine Capped ZnS Nanoparticles. *Inorg. Chim. Acta,* **2017**, *463*, 7-13

(10) (a) Nyman, M.; Hampden-Smith, M. J.; Duesler, E. N. Low Temperature, Aerosol-Assisted Chemical Vapor Deposition (AACVD) of CdS, ZnS, and $Cd_{1-x}Zn_xS$ Using Monomeric Single-Source Precursors: M(SOCCH$_3$)$_2$:TMEDA. *Chem. Vap. Deposition,* **1996**, *2*, 171-174; (b) Vittal, J. J.; Ng, M. T. Chemistry of Metal Thio- and Selenocarboxylates: Precursors for Metal Sulfide/Selenide Materials, Thin Films, and Nanocrystals. *Acc. Chem. Res.,* **2006**, *39*, 869-877; (c) Vallejo-Sánchez, D.; Beobide, G.; Castillo, O.; Lanchas, M. Zinc Thiocarboxylate Complexes as Precursors for Zinc Sulfide Nanoparticles under Aerobic Conditions. *Eur. J. Inorg. Chem.,* **2013**, *32*, 5592-5602

(11) Byrom, C.; Malik, M. A.; O'Brien, P.; White, A. J. P.; Williams, D. J. Synthesis and X-ray Single Crystal Structures of Bis(diisobutyldithiophosphinato)Cadmium(II) or Zinc(II): Potential Single-Source Precursors for II/VI Materials. *Polyhedron,* **2000**, *19*, 211-215

(12) Rojas-Montoya, I. D.; Santana-Silva, A.; García-Montalvo, V.; Muñoz-Hernández, M.-Á.; Rivera, M. N-(Chalcogen)phosphorylated (Chalcogen)ureas of Zinc and Cadmium(ii): SSPs for Group 12–16 Thin Films. *New J. Chem.,* **2014**, *38*, 4702-4710

(13) (a) Ramasamy, K.; Malik, M. A.; O'Brien, P.; Raftery, J. Metal Complexes of Thiobiurets and Dithiobiurets: Novel Single Source Precursors for Metal Sulfide Thin Film Nanostructures. *Dalton Trans.,* **2010**, *39*, 1460-1463; (b) Ramasamy, K.; Malik, M. A.; Helliwell, M.; Raftery, J.; O'Brien, P. Thio- and Dithio-Biuret Precursors for Zinc Sulfide, Cadmium Sulfide, and Zinc Cadmium Sulfide Thin Films. *Chem. Mater.,* **2011**, *23*, 1471-1481; (c) Abdelhady, A. L.; Malik, M. A.; O'Brien, P. Colloidal Synthesis of ZnS, CdS and Zn x Cd1−x S Nanoparticles from Zinc and Cadmium Thiobiuret Complexes. *J. Inorg. Organomet. Polym. Mater.,* **2013,** *24*, 226-240

(14) (a) Maury, F. Trends in Precursor Selection for MOCVD. *Chem. Vap. Deposition,* **1996**, *2*, 113-116; (b) Afzaal, M.; Malik, M. A.; O'Brien, P. Chemical Routes to Chalcogenide Materials as Thin Films or Particles with Critical Dimensions with the Order of Nanometres. *J. Mater. Chem.,* **2010**, *20*, 4031-4040

(15) Gleizes, A. N. MOCVD of Chalcogenides, Pnictides, and Heterometallic Compounds from Single-Source Molecule Precursors. *Chem. Vap. Deposition,* **2000**, *6*, 155-173

(16) Marchand, P.; Hassan, I. A.; Parkin, I. P.; Carmalt, C. J. Aerosol-Assisted Delivery of Precursors for Chemical Vapour Deposition: Expanding the Scope of CVD for Materials Fabrication. *Dalton Trans.,* **2013**, *42*, 4906-9422
(17) (a) Pike, R. D.; Cui, H.; Kershaw, R.; Dwight, K.; Wold, A.; Blanton, T. N.; Wernberg, A. A.; Gysling, H. J. Preparation of Zinc Sulfide Thin Films by Ultrasonic Spray Pyrolysis from Bis(diethyldithiocarbamato) Zinc(II). *Thin Solid Films,* **1993**, *224*, 221-226; (b) Nomura, R.; Murai, T.; Toyosaki, T.; Matsuda, H. Single-Source MOVPE Growth of Zinc Sulfide Thin Films using Zinc Dithiocarbamate Complexes. *Thin Solid Films,* **1995**, *271*, 4-7
(18) Knapp, C. E.; Carmalt, C. J. Solution Based CVD of Main Group Materials. *Chem. Soc. Rev.,* **2016**, *45*, 1036-1064
(19) Buckingham, M. A.; Catherall, A. L.; Hill, M. S.; Johnson, A. L.; Parish, J. D. Aerosol-Assisted Chemical Vapor Deposition of CdS from Xanthate Single Source Precursors. *Cryst. Growth Des.,* **2017**, *17*, 907-912
(20) Powell, M. J.; Carmalt, C. J. Aerosols: A Sustainable Route to Functional Materials. *Chem. Eur. J.,l* **2017**, *23*, 15543-15552
(21) Catherall, A. L.; Harris, S.; Hill, M. S.; Johnson, A. L.; Mahon, M. F. Deposition of SnS Thin Films from Sn(II) Thioamidate Precursors. *Cryst. Growth Des.,* **2017**, *17*, 5544-5551
(22) Ahmet, I. Y.; Hill, M. S.; Johnson, A. L.; Peter, L. M. Polymorph-Selective Deposition of High Purity SnS Thin Films from a Single Source Precursor. *Chem. Mater.,* **2015**, *27*, 7680-7688
(23) Schmidt, S.; Schulz, S.; Bolte, M. $[^{t}BuC(N^{i}Pr)_2]_2Zn$ as Starting Reagent for Monoamidinate Zinc Complexes $\{[^{t}BuC(N^{i}Pr)_2]ZnX\}_2$. *Z. Anorg. Allg. Chem.,* **2009**, *635*, 2210-2213
(24) Willdsmith, T.; Hill, M. S.; Johnson, A. L.; Kingsley, A. J.; Molloy, K. C. Exclusive Formation of SnO by Low Temperature Single-Source AACVD. *Chem. Commun.,* **2013**, *49*,
(25) (a) Kanters, J. A.; Spek, A. L.; Postma, R.; van Stein, G. C.; van Koten, G. Structure of Bis[N-(2-pyrrolylmethylene)-tert-butylamine]Zinc(II), $Zn(C_9H_{13}N_2)_2$. *Acta Cryst. Sec. C: Cryst. Struct. Commun.,* **1983**, *39*, 999-1001; (b) Fernández-Galán, R.; Antiñolo, A.; Carrillo-Hermosilla, F.; López-Solera, I.; Otero, A.; Serrano-Laguna, A.; Villaseñor, E. Migratory Insertion Reactions in Asymmetrical Guanidinate-Supported Zirconium Complexes. *Organometallics* **2012**, *31*, 8360-8369
(26) Johnson, A. L.; Hollingsworth, N.; Kociok-Köhn, G.; Molloy, K. C. Organozinc Aminoalcoholates: Synthesis, Structure, and Materials Chemistry. *Inorg. Chem.,* **2008**, *47*, 12040-12048
(27) Coles, Martyn P.; Hitchcock, Peter B. Zinc Guanidinate Complexes and Their Application in Ring-Opening Polymerisation Catalysis. *Eur. J. Inorg. Chem.,* **2004**, *13*, 2662-2672
(28) (a) Benson, R. E.; Ellis, C. A.; Lewis, C. E.; Tiekink, E. R. T. 3D-, 2D- and 1D-Supramolecular Structures of $\{Zn[S_2CN(CH_2CH_2OH)R]_2\}_2$ and their $\{Zn[S_2CN(CH_2CH_2OH)R]_2\}_2$(4,4′-bipyridine) Adducts for R = CH_2CH_2OH, Me or Et: Polymorphism and Pseudo-Polymorphism. *Cryst. Eng. Comm.,* **2007**, *9*, 930-940; (b) Malik, M. A.; Obrien, P. Mixed Methyl-Zinc and Ethylzinc Complexes with Diethylselenocarbamate - Novel Precursors for ZnSe. *Chem. Mater.* **1991**, *3*, 999-1000; (c) Memon, A. A.; Afzaal, M.; Malik, M. A.; Nguyen, C. Q.; O'Brien, P.; Raftery, J. The N-alkyldithiocarbamato Complexes $[M(S_2CNHR)_2]$ (M = Cd(II) Zn(II); R = C_2H_5, C_4H_9, C_6H_{13}, $C_{12}H_{25}$); Their synthesis, thermal Decomposition and use to Prepare of Nanoparticles and Nanorods of CdS. *Dalton Trans.,* **2006**, (37), 4499-4505; (d) O'Brien, P.; Walsh, J. R.; Watson, I. M.; Motevalli, M.; Henriksen, L. Novel Dithio- and Diseleno-Carbamates of Zinc and Cadmium as Single-Molecule Precursors for Low-

Pressure Metal-Organic Chemical Vapour Deposition. *J. Chem. Soc., Dalton Trans.,* **1996**, *12*, 2491-2496
(29) Drdácký, M.; Lesák, J.; Rescic, S.; Slížková, Z.; Tiano, P.; Valach, J. Standardization of Peeling Tests for Assessing the Cohesion and Consolidation Characteristics of Historic Stone Surfaces. *Mater. Struct.,* **2011**, *45*, 505-520
(30) Kole, A. K.; Kumbhakar, P. Cubic-to-Hexagonal Phase Transition and Optical Properties of Chemically Synthesized ZnS Nanocrystals. *Res. Phys.,* **2012**, *2*, 150-155
(31) (a) Xiong, Q. H.; Wang, J. G.; Reese, O.; Voon, L.; Eklund, P. C. Raman Scattering from Surface Phonons in Rectangular Cross-Sectional W-ZnS Nanowires. *Nano Lett.,* **2004**, *4*, 1991-1996; (b) Nilsen, W. G. Raman Spectrum of Cubic ZnS. *Phys. Rev.,* **1969**, *182*, 838-850; (c) Kim, J. H.; Rho, H.; Kim, J.; Choi, Y. J.; Park, J. G. Raman Spectroscopy of ZnS Nanostructures. *J. Raman Spectrosc.,* **2012**, *43*, 906-910; (d) Cheng, Y. C.; Jin, C. Q.; Gao, F.; Wu, X. L.; Zhong, W.; Li, S. H.; Chu, P. K. Raman Scattering Study of Zinc Blende and Wurtzite ZnS. *J. Appl. Phys.,* **2009**, *106*, 123505-1-123505-5
(32) Vallejos, S.; Umek, P.; Blackman, C. Aerosol Assisted Chemical Vapour Deposition Control Parameters for Selective Deposition of Tungsten Oxide Nanostructures. *J. Nanosci. Nanotech.,* **2011**, *11*, 8214-8220
(33) Vallejos, S.; Selina, S.; Annanouch, F. E.; Gràcia, I.; Llobet, E.; Blackman, C. Aerosol Assisted Chemical Vapour Deposition of Gas sensitive SnO_2 and Au-Functionalised SnO_2 Nanorods via a Non-Catalysed Vapour Solid (VS) Mechanism. *Sci Rep.,* **2016**, *6*, 1-12
(34) (a) Madugu, M. L.; Olusola, O. I.-O.; Echendu, O. K.; Kadem, B.; Dharmadasa, I. M. Intrinsic Doping in Electrodeposited ZnS Thin Films for Application in Large-Area Optoelectronic Devices. *J. Electron. Mater.,* **2016**, *45*, 2710-2717; (b) Yoo, D.; Choi, M. S.; Heo, S. C.; Chung, C.; Kim, D.; Choi, C. Structural, Optical and Chemical Analysis of Zinc Sulfide Thin Film Deposited by RF-Mganetron Sputtering and Post Deposition Annealing. *Met.Mater. Int.,* **2013**, *19*, 1309-1316
(35) (a) Yoon, Y. G.; Choi, I. H. Preparation of ZnS Thin Films by Using Photoassisted MOCVD. *J. Korean Phys. Soc.,* **2013**, *63*, 1609-1614; (b) Xu, H.; Li, Y.; Rosa, A. L.; Frauenheim, T.; Zhang, R. Q. First-Principles Study of the Structural Stability and Electronic Properties of ZnS Nanowires. *J. Phys. Chem. C,* **2008**, *112*, 20291-20294; (c) Wei, A. X.; Liu, J.; Zhuang, M. X.; Zhao, Y. Preparation and Characterization of ZnS Thin Films Prepared by Chemical Bath Deposition. *Mater. Sci. Semicond. Process.,* **2013**, *16*, 1478-1484; (d) Schrier, J.; Demchenko, D. O.; Wang, L. W. Optical properties of ZnO/ZnS and ZnO/ZnTe Heterostructures for Photovoltaic Applications. *Nano Lett.,* **2007**, *7*, 2377-2382 ; (e) Li, Z. Q.; Shi, J. H.; Liu, Q. Q.; Wang, Z. A.; Sun, Z.; Huang, S. M. Effect of Zn / S Ratios on the Properties of Chemical Bath Deposited Zinc Sulfide Thin Films. *Applied Surface Science* **2010**, *257*, 122-126; (f) Fang, X. S.; Zhai, T. Y.; Gautam, U. K.; Li, L.; Wu, L. M.; Yoshio, B.; Golberg, D. ZnS Nanostructures: From Synthesis to Applications. *Prog. Mater. Sci.,* **2011**, *56*, 175-287
(36) Rivillo, D.; Gulyás, H.; Benet-Buchholz, J.; Escudero-Adán, E. C.; Freixa, Z.; van Leeuwen, P. W. N. M. Catalysis by Design: Wide-Bite-Angle Diphosphines by Assembly of Ditopic Ligands for Selective Rhodium-Catalyzed Hydroformylation. *Angew. Chem. Int. Ed.,* **2007**, *46*, 7247-7250

Table of Content Abstract and Graphic

We report the synthesis and characterization of a family of Zinc(II) thoureide complexes, of the general form [{**L**}ZnMe], [{**L**}Zn{N(SiMe$_3$)$_2$}] and [{**L**}$_2$Zn]. Thermogravimetric analysis has been used to assess the viability of complexes **1-12** as single source precursors for the formation of ZnS. On the basis of TGA data compound **9**, [{**L**^{1}}$_2$Zn] was investigated for its utility as a single source precursor to deposit ZnS films on silica-coated glass and crystalline silicon substrates at 150, 200, 250 and 300 °C respectively using an aerosol assisted chemical vapour deposition (AACVD). Analysis of the thin films by SEM and AFM Raman and UV-Vis spectroscopy reveal the films to be hexagonal (Wurtzite) W-ZnS.